Journal of Experimental Botany, Vol. 70, No. 21 pp. 6163–6179, 2019
doi:10.1093/jxb/erz391 Advance Access Publication September 6, 2019
This paper is available online free of all access charges (see https://academic.oup.com/jxb/pages/openaccess for further details)

RESEARCH PAPER

Pentatricopeptide repeat protein DEK45 is required for mitochondrial function and kernel development in maize

Ru Chang Ren[1], Xiaoduo Lu[2], Ya Jie Zhao[1], Yi Ming Wei[1], Li Li Wang[1], Lin Zhang[1], Wen Ting Zhang[1], Chunyi Zhang[3], Xian Sheng Zhang[1,*], and Xiang Yu Zhao[1,*]

[1] State Key Laboratory of Crop Biology, College of Life Sciences, Shandong Agricultural University, Taian, Shandong 271018, China
[2] Institute of Molecular Breeding for Maize, Qilu Normal University, Jinan 250200, China
[3] Biotechnology Research Institute, Chinese Academy of Agricultural Sciences, Beijing 100081, China

* Correspondence: zhxy@sdau.edu.cn or zhangxs@sdau.edu.cn

Received 1 April 2019; Editorial decision 13 August 2019; Accepted 15 August 2019

Editor: Gerhard Leubner, Royal Holloway, University of London, UK

Abstract

Pentatricopeptide repeat (PPR) proteins are one of the largest protein families, which consists of >400 members in most species. However, the molecular functions of many PPR proteins are still uncharacterized. Here, we isolated a maize mutant, *defective kernel 45* (*dek45*). Positional cloning, and genetic and molecular analyses revealed that DEK45 encodes a new E+ subgroup PPR protein that is localized in the mitochondrion. DEK45 recognizes and directly binds to *cox3*, *nad2*, and *nad5* transcripts and functions in their processing. In the *dek45* mutant, abolishment of the C-to-U editing of *cox3*-314, *nad2*-26, and *nad5*-1916 leads to accumulated reactive oxygen species and promoted programmed cell death in endosperm cells due to the dysfunction of mitochondrial complexes I and IV. Furthermore, RNA sequencing analysis showed that gene expression in some pathways, such as glutathione metabolism and starch biosynthesis, was altered in the *dek45* mutant compared with the wild-type control, which might be involved in abnormal development of the maize mutant kernels. Thus, our results provide solid evidence on the molecular mechanism underlying RNA editing by DEK45, and extend our understanding of PPR-E+ type protein in editing functions and kernel development in maize.

Keywords: Kernel development, maize, mitochondrion, pentatricopeptide repeat protein, RNA editing.

Introduction

RNA editing mediated by organellar genes at the transcript level is an essential step in the production of functional proteins (Castandet and Araya, 2011). Most RNA editing events are conversions of cytidines (C) to uridines (U) in mitochondria or plastids (Ichinose and Sugita, 2017). These RNA modification processes are mostly regulated by nuclear-encoded factors (Takenaka *et al.*, 2013b; Ichinose and Sugita, 2017). Interestingly, many RNA-binding proteins, such as pentatricopeptide repeat (PPR) proteins, function in RNA post-transcriptional processes in organelles (Fujii and Small, 2011; Barkan and Small, 2014).

PPR proteins are characterized by tandem repeats of a highly degenerate 35 amino acid motif (Small and Peeters, 2000). They are found in all eukaryotes, but their numbers are greatly increased in land plants (Schmitz-Linneweber and Small, 2008; Takenaka *et al.*, 2014). Based on the structure of their PPR motifs, PPR proteins are divided into two categories, the P subfamily and the PLS subfamily (Lurin

et al., 2004). The PLS subfamily proteins are further divided into four subgroups, PLS, E, E+, and DYW, according to their C-terminal motifs (Lurin et al., 2004). The PPR motif contains two antiparallel α-helices (helix A and helix B), which interact to form a superhelix as a helix–turn–helix motif (Small and Peeters, 2000;Yin et al., 2013). RNA substrates of PPR proteins can be identified in a motif sequence-specific manner. Positions 6 and 1′ (position 1 in the next motif) or positions 4′ and 34′ in the PPR motif are responsible for RNA binding and nucleotide recognition (Barkan et al., 2012; Takenaka et al., 2013*a*; Yin et al., 2013). All three types of PPR proteins, the E, E+, and DYW subgroups, are involved in mitochondrial or plastid RNA editing (Fujii and Small, 2011; Barkan and Small, 2014; Li et al., 2014; Sun et al., 2015;Yang et al., 2017; Li et al., 2019). Defects in these proteins lead to phenotypes associated with organelle dysfunction, such as embryo developmental arrest, embryo lethality, albino plants, cytoplasmic male sterility, and poor growth (Saha et al., 2007; Schmitz-Linneweber and Small, 2008).

The plant respiratory chain is composed of four main complexes and an ATP synthase (Dudkina et al., 2006). These four main complexes comprise complex I (NADH-ubiquinone oxidoreductase), complex II (succinate-ubiquinone oxidoreductase), complex III (ubiquinol-cytochrome *c* oxidoreductase), and complex IV (cytochrome *c*-O_2 oxidoreductase). In the mitochondrial electron transport chain (ETC), complexes I and III can catalyze reactive oxygen species (ROS) formation under physiological and pathological conditions (Blokhina and Fagerstedt, 2010; Gill and Tuteja, 2010). Impaired complex I activity in the mitochondrial ETC results in redox imbalance and increased ROS accumulation (Liu et al., 2010; Xie et al., 2016; Lee et al., 2017). The defective cytochrome *c* pathway in the *ppr40* mutant enhanced ROS accumulation (Zsigmond et al., 2008). ROS not only are important signaling molecules that regulate and coordinate vital processes including growth, the cell cycle, programmed cell death (PCD), abiotic stress responses, defense, systemic signaling, and development, but they also control protein stability and gene expression (Laloi et al., 2004; Gechev et al., 2006). Besides the cytochrome oxidase (COX) pathway, the alternative oxidase (AOX) pathway represents an alternative electron transport pathway in mitochondrial ETC (Vanlerberghe, 2013). When electron transport in the cytochrome *c* pathway is blocked, mitochondrial dysfunction signaling up-regulates the expression of *AOX* genes, which regulate the ROS levels initiated by mitochondrial retrograde signaling (Zsigmond et al., 2008).

In this study, DEK45, a new maize E+ type PPR protein was identified, which directly binds to *cox3*, *nad2*, and *nad5* transcripts. Its dysfunction abolished the C-to-U editing of *cox3*-314, *nad2*-26, and *nad5*-1916, impaired mitochondrial complex I and IV activity, and promoted ROS accumulation and PCD of endosperm cells. Gene expression profile analysis demonstrated that some biosynthesis and metabolism pathways were altered in the *dek45* mutant, for example glutathione metabolism and starch biosynthesis pathways, which might be involved in abnormal development of the maize kernels.

Materials and methods

Plant materials

The maize *dek45-reference* (*dek45-ref*) mutant was isolated from an ethyl methanesulfonate (EMS) population (in the B73 genetic background). The second allele *dek45-1* was obtained from the MEMD website (Maize EMS-induced Mutant Database, http://www.elabcaas.cn/memd/; last accessed 8 September 2019) (Lu et al., 2018). The *dek45-ref* allele was maintained in heterozygotes and the *dek45-ref* mutant was backcrossed to B73 to generate BC_3F_1; BC_3F_2 seeds were used for further experiments. The *dek45-ref* heterozygotes were used as male parents in crosses with four inbred lines, Mo17,V3b1, Chang7-2, and S162.The wild-type (WT) plants used in this study were siblings of the mutant from self-pollinated segregating ears.Arabidopsis (*Arabidopsis thaliana*) line MT-GK (CS16263) used for subcellular localization analysis of DEK45 was obtained from the Arabidopsis Biological Resource Center.

Histological analysis

Kernels at different days after pollination (DAP) were cut longitudinally into three equal parts. The central part containing the intact embryo was fixed with formalin–acetic acid–alcohol (FAA) solution (50 ml of 100% ethanol, 10 ml of glacial acetic acid, 5 ml of 37% formaldehyde, and 35 ml of ddH_2O) for 12–14 h at 4 °C. The fixed material was dehydrated in a graded ethanol series (50, 70, 85, 95, and 100%), which was subsequently replaced with xylene, and infiltrated with paraffin. The samples were embedded and cut into 12 μm sections using an RM2235 microtome (Leica, Wetzlar, Germany). The sections were stained with 0.1% (w/v) Toluidine Blue O (Sigma-Aldrich, USA). Finally, photographs were taken using a microscope (Olympus BX51).

TEM and SEM

For TEM analysis, immature WT and *dek45-ref* endosperm at 11 and 13 DAP was collected from the same ear, cut into small pieces, and fixed with 2.5% glutaraldehyde and 1% osmium tetroxide at 4 °C for 12 h. The samples were subsequently washed five times with phosphate-buffered saline (PBS; pH 7.2). After dehydration in an ethanol gradient, they were transferred to propylene epoxide and gradually infiltrated with acrylic resin. Ultrathin sections of the samples were cut with a diamond knife and photomicrographs were taken using a transmission electron microscope (JEM-1400Plus) at Shandong Agricultural University.

For SEM analysis, mature WT and *dek45-ref* seeds were harvested from the same ear and cut longitudinally with a knife. The samples were vacuum-dried, spray-coated with gold, and observed using a scanning electron microscope (JSM-6610LV) at Shandong Agricultural University.

Map-based cloning

The *Dek45* locus was mapped using 702 mutant individuals from an F_2 mapping population of the cross between *dek45-ref* heterozygotes and the S162 inbred line. For preliminary mapping, >100 polymorphic simple sequence repeat (SSR) markers evenly distributed over the whole genome were selected to analyze both parents and F_2 mutant kernels. For fine mapping, molecular markers were developed based on single nucleotide polymorphisms (SNPs), SSRs, and Indels. The molecular markers narrowed the *Dek45* locus down to a 300 kb region. Based on candidate gene annotation in this region, DNA fragments were amplified from 10 *dek45-ref* and WT kernels using KOD DNA polymerase (Toyobo) and sequenced. The primer sequences are listed in Supplementary Table S4 at *JXB* online.

Phylogenetic analysis

All the sequences were aligned with the MAFFT program (Katoh et al., 2002). The phylogenetic trees were reconstructed by the maximum likelihood (ML) method implemented in IQ-TREE, with the best-fit model automatically selected by ModelFinder. Support for the inferred ML tree

was obtained by ultrafast bootstrap approximation (UFBoot) with 10 000 replicates (Nguyen *et al.*, 2015; Kalyaanamoorthy *et al.*, 2017). Figtree was used for visualization (Figtree v1.4.4 visualization; http://tree.bio.ed.ac.uk/software/figtree/; last accessed 8 September 2019).

DNA isolation and RNA extraction

Genomic DNA (gDNA) for each sample was isolated from mature maize kernels without pericarp using the GMO Crop Extraction & Amplification kit (Tiangen, Beijing, China) following the manufacturer's instructions. Total RNA of developing kernels was extracted using a cetyltrimethylammonium bromide (CTAB)-based method (Gambino *et al.*, 2008). Total RNA of other samples was extracted using the Trizol reagent (Ambion; Cat. No. 15596-026).

Reverse transcription-PCR (RT–PCR) and quantitative RT–PCR (qRT–PCR)

Total RNA was treated with gDNA buffer to remove residual DNA contamination and reverse transcribed to cDNA using a FastQuant RT Kit (Tiangen). RT–PCR was used to examine RNA editing, and the products were introduced into the *pEAZY*-Blunt3 Cloning vector (Tiangen) and directly sequenced. Amplification of mitochondrial transcripts was performed using primers as described previously (Liu *et al.*, 2013).

qRT–PCR was performed with cDNA dilutions using SuperReal PreMix Plus (Tiangen) with a LightCycler 96 (Roche Diagnostics) in a 20 µl reaction volume with 45 cycles. The RNA levels were normalized to the maize *ZmActin* gene (GRMZM2G126010) with three biological replicates, and three technical replicates each. The primers used for qRT–PCR are listed in Supplementary Table S4.

Subcellular localization

The full-length coding sequence of *Dek45* without the termination codon was amplified with specific primers and cloned into the pROKII-GFP vector to generate a green fluorescent protein (GFP) fusion product. The modified subcellular localization assays were conducted according to the method described by Yoo *et al.* (2007). Briefly, 0.5–1 mm leaf strips were cut from etiolated leaves at 14 d after sowing and digested with 1.5% (w/v) cellulase R10 and 0.5% (w/v) macerozyme R10 (Yakult Pharmaceutical Ind. Co., Ltd, Japan). The digestion continued for 5 h at room temperature with 50 rpm shaking in the dark. The DEK45–GFP fusion products were transfected into maize protoplasts by polyethylene glycol/calcium-mediated transformation (Yoo *et al.*, 2007). The protoplasts were incubated for 14–18 h in the dark at 23 °C. After incubation, the protoplasts were treated with 500 nM of the mitochondrion-selective dye Mito Tracker Red CMX-Ros (Invitrogen) for 30 min at 37 °C, and washed with W5 solution three times. DEK45–GFP and Mito Tracker Red CMX-Ros were excited at 488 nm and 561 nm, and emissions were collected at 505–550 nm and 575–615 nm, respectively. Images were captured using a Leica TCS SP5 II laser scanning confocal microscope. The subcellular localization of DEK45–red fluorescent protein (RFP) in the Arabidopsis marker line for mitochondria (MT-GK) was performed as described previously (Zhang *et al.*, 2018). Primer sequences are listed in Supplementary Table S4.

Measurement of ROS in endosperms

Developing WT and *dek45-ref* mutant kernels were isolated from self-pollinated segregating ears at 11, 13, and 15 DAP, and used to measure ROS in the endosperms. For 3,3'-diaminobenzidine (DAB) staining to detect hydrogen peroxide (H_2O_2), the kernels were cut longitudinally into two equal parts and placed in 1 mg ml^{-1} DAB (Sigma-Aldrich) in 50 mM Tris–HCl buffer (pH 5.0) in the dark for 12 h. For nitroblue tetrazolium chloride (NBT) staining to detect superoxides, the kernels were cut, immersed in a 0.5 mg ml^{-1} NBT (Sigma-Aldrich) solution in 10 mM potassium phosphate buffer (pH 7.6), and incubated in complete darkness at room temperature for 2 h. After each assay, the kernels were fixed in 70% (v/v) ethanol at room temperature. Photographs were taken using an Olympus DP72 microscope. The relative DAB and NBT staining intensities were analyzed with the Image J software.

Terminal deoxynucleotidyl transferase dUTP nick end labeling (TUNEL) assays

The TUNEL assay was performed as described previously (Wang *et al.*, 2014). Kernels were fixed in formaldehyde solution overnight at 4 °C, embedded in paraffin after dehydration, and sectioned at 12 µm thickness. The sections were dewaxed in xylene, rehydrated in an ethanol series, treated with 20 µg ml^{-1} Proteinase K (Gibco, Carlsbad, CA, USA) in Proteinase K buffer (10 mM Tris–HCl and 5 mM EDTA, pH 7.5) for 15 min at 37 °C, and washed with PBS solution twice. The samples were incubated in a mixture of fluorescein-labeled deoxynucleotides and TdT (TUNEL mix) at 37 °C for 1 h. After incubation, the slides were washed with PBS solution, treated with 10 µg ml^{-1} propidium iodide (PI) for 15 min at 37 °C, and washed again with PBS solution. The samples were observed using a Leica TCS SP5 II laser scanning confocal microscope.

RNA EMSAs

The full-length coding sequence of *Dek45* was amplified with specific primers and cloned into the pGEX-4T-1 vector to generate recombinant DEK45–glutathione *S*-transferase (GST). The DEK45–GST construct was expressed in the *Escherichia coli* BL21 (DE3) cell line. DEK45 tagged with GST was purified using glutathione Sepharose 4B (GE Healthcare). Two RNA probes for *cox3*-314, *nad2*-26, and *nad5*-1916 were synthesized and labeled with biotin at the 3′ end. The LightShift Chemiluminescent RNA EMSA Kit (Thermo Scientific; catalog no. 20158) was used for binding reactions and labeled complex detection following the manufacturer's instructions. Competition experiments were performed with different concentrations of unlabeled probe. The primer sequences are listed in Supplementary Table S4.

Isolation and analysis of mitochondrias complexes

Mitochondria for blue native PAGE (BN-PAGE) and complex activity analysis were isolated from kernels without pericarp of self-pollinated segregating ears at 15 DAP as described previously (Chen *et al.*, 2017). The enriched mitochondria were resuspended in 40 µl of sample buffer [50 mM Bis-Tris, 6 N HCl, 50 mM NaCl, 10% (w/v) glycerol, 0.001% Ponceau S] with 20% *n*-dodecyl-β-D-maltoside added to a final concentration of 1%, and incubated for 30 min on ice. The samples were centrifuged at 20 000 *g* for 30 min at 4 °C and loaded on native PAGE Novex 4–16% Bis-Tris gels (Invitrogen, BN1002BOX). The electrophoresis was performed following the manufacturer's protocol. The gels were stained with Coomassie Blue R-250 (Sigma-Aldrich). The activities of mitochondrial complexes were determined by colorimetry as described previously (Luo *et al.*, 2008; Muhling *et al.*, 2010; Gadicherla *et al.*, 2012).

RNA sequencing (RNA-seq) and data analysis

Total RNAs were extracted from the endosperm of WT and *dek45-ref* at 10 DAP using the CTAB-based method. Two biological repeats (8–10 individuals per pool) of WT (WT-A, WT-B) and *dek45-ref* (dek-A, dek-B) were isolated from two different segregating ears, and used for RNA-seq. High-throughput sequencing was performed on the Illumina HiSeq4000 platform at the Beijing Genomics Institute (BGI; Shenzhen, China). After sequencing, reads of low quality, adaptor polluted, and with a high content of unknown bases (N) were filtered to obtain clean reads, and these clean reads were then mapped to the reference genome (http://www.maizegdb.org/; last accessed 8 September 2019, *Zea mays*.AGPv3) using HISAT (Kim *et al.*, 2015). For gene expression analysis, clean reads were mapped to the reference using Bowtie2 (Langmead and Salzberg, 2012) and then the gene expression level was calculated with RSEM (Li and Dewey, 2011). We determined differentially expressed genes (DEGs) as described {[fold change ≥2.00 and –log10 (1–probability) ≥0.8] and [fold change ≥2.00 and false discovery rate (FDR) ≤0.001]}. RNA-seq data are

available from the National Center for Biotechnology Information Gene Expression Omnibus (http://www.ncbi.nlm.nih.gov/geo; last accessed 8 September 2019) under the series entry GEO: GSE122962.

Results

Genetic and phenotypic characterization of the dek45 *mutant*

A defective kernel mutant was isolated from an EMS mutant library of inbred line B73 and designated *dek45-ref*. Self-pollinated *dek45-ref* heterozygotes produced ~25% defective kernels (defective kernel number/total kernel number=292/1211, P=0.48). To confirm this segregation, we crossed *dek45-ref* heterozygotes to each of four maize inbred lines, S162, V3b1, Mo17, and Chang7-2. Among these monohybrid crosses, ~50% (106/209) of the first generation (F_1) had phenotype-segregating ears, which matched the 1:1 segregation ratio. Moreover, the ratio of WT to mutant phenotype kernels in the second-generation (F_2) offspring of the segregating ears was 3:1 in all four genetic backgrounds (Supplementary Table S1). Thus, a monogenic recessive mutation was responsible for the phenotype of *dek45-ref*.

A germination test showed that *dek45-ref* kernels could not geminate, indicating embryo lethality. Therefore, the *dek45-ref* allele was maintained with heterozygotes. On self-pollinated heterozygous ears at 15 and 25 DAP, the *dek45-ref* mutant kernels displayed small, white, and translucent phenotypes (Fig. 1A, B). Longitudinal dissection of WT and mutant sibling kernels from segregated ears at 15 and 25 DAP showed that kernels with the WT phenotype contained starch-filled endosperm and normal embryos, while *dek45-ref* kernels had a soft texture and abnormal embryos (Fig. 1C–F). Moreover, there was a cavity in the central region of the *dek45-ref* mutant endosperm at 25 DAP (Fig. 1F). In the frontal view, both the mutant kernel and embryo were smaller than in the WT (Fig. 1G). The 100-kernel weight of *dek45-ref* was nearly 82.4% less than that of the WT (Fig. 1H), indicating that *dek45-ref* kernel development was severely defective.

Due to the dramatic *dek45-ref* kernel defects, we analyzed embryo and endosperm development of *dek45-ref* and WT kernels at 7–25 DAP from the same segregating ear using histological sections (Fig. 1I–L; Supplementary Fig. S1). The mutant kernels exhibited developmental delay compared with WT kernels. At 15 DAP, the WT pericarp was filled with endosperm, and the embryo had developed an obvious scutellum, coleoptile, two leaf primordia, and both shoot and root apical meristems (Fig. 1I). However, the mutant kernel embryo had only a coleoptile and an empty space between the pericarp and the endosperm (Fig. 1J). At 25 DAP, the WT embryos were larger and produced five or six leaf primordia (Fig. 1K); in contrast, the mutant kernel embryos remained small and had a shoot apical meristem-like structure with one or two tiny leaf primordia (Fig. 1L). These results indicated that embryo and endosperm development was arrested in *dek45-ref* kernels.

Further analysis showed an obvious difference in starch accumulation between mutant and WT endosperm cells. As shown in Fig. 2A–F, WT kernels accumulated many starch granules, while mutant kernels contained fewer starch granules. Longitudinal dissection of WT and *dek45-ref* dry seeds showed that the ratio of hard to soft endosperm was decreased in *dek45-ref* (Fig. 2G). SEM analysis revealed that the starch granules in the peripheral hard endosperm cells were tightly packed in the WT (Fig. 2H), but loosely packed in *dek45-ref* (Fig. 2J). The central starchy endosperm cells were filled with irregular polyhedrons and large starch granules in the *dek45-ref* endosperm (Fig. 2I, K). In addition, protein body accumulation appeared to be reduced in the central endosperm cells of *dek45-ref* compared with those in the WT (Fig. 2I, K).

Positional cloning of Dek45

To identify the locus responsible for the *dek45-ref* mutant phenotype, an F_2 mapping population from a cross between *dek45-ref* heterozygotes and the WT inbred line S162 were used for map-based cloning of the candidate gene. Through analysis of 48 mutant individuals, the *Dek45* gene was mapped between the SSR markers umc1380 and umc1152 on the short arm of chromosome 10 (Fig. 3A). To narrow down the location of *Dek45*, we selected eight polymorphic markers (Supplementary Table S4) to screen 702 mutant individuals. Finally, the *Dek45* locus was mapped to a 300 kb region between molecular markers M4 and M5. Eight candidate genes were identified in this region (Fig. 3A). DNA sequence comparison of these candidate genes between WT and mutant alleles revealed two SNPs in two adjacent genes. One was a putative PPR gene whose SNP mutation (G to A) at base pair +1719 resulted in an amino acid replacement (Gly to Arg) (Fig. 3A, B), and the other was a putative WRKY transcription factor and its SNP transition (G to A) at base pair +262 caused an Arg to Lys substitution (Fig. 3A).

To determine which mutation was responsible for the *dek45-ref* phenotype, we examined co-segregation between the mutation sites and the *dek45-ref* mutant phenotypes by PCR and DNA sequencing in 158 WT phenotype individuals that were segregated from the self-progenies of *dek45-ref* heterozygotes. Only the self-progenies of the individuals with a heterozygote mutation (GA) in the PPR gene were segregated (Supplementary Table S2), suggesting that the SNP mutation (G to A) at base pair +1719 in the gene GRMZM2G304965 was the locus responsible for the *dek45-ref* phenotypes. Thus, the gene was named *Dek45*.

To confirm that the candidate PPR gene was the gene responsible for the *dek45-ref* phenotypes, we identified another mutant allele of this gene designated *dek45-1*. *dek45-1* had an SNP mutation (G to A) at base pair +2180, resulting in a premature stop codon in the mature transcript (Fig. 3B, C). The self-progenies of *dek45-1* heterozygotes produced similar defective kernels to *dek45-ref* in a recessive pattern (Fig. 3D). Crosses between *dek45-ref* and *dek45-1* heterozygotes produced defective kernels, with ears segregating with normal and defective kernels in an expected 3:1 ratio, demonstrating that they were allelic (Fig. 3D). The results were further confirmed by PCR sequencing genotyping (Supplementary Table S3). Additionally, histological analysis of WT and *dek45-1* kernels at 15 DAP showed that embryo and endosperm development

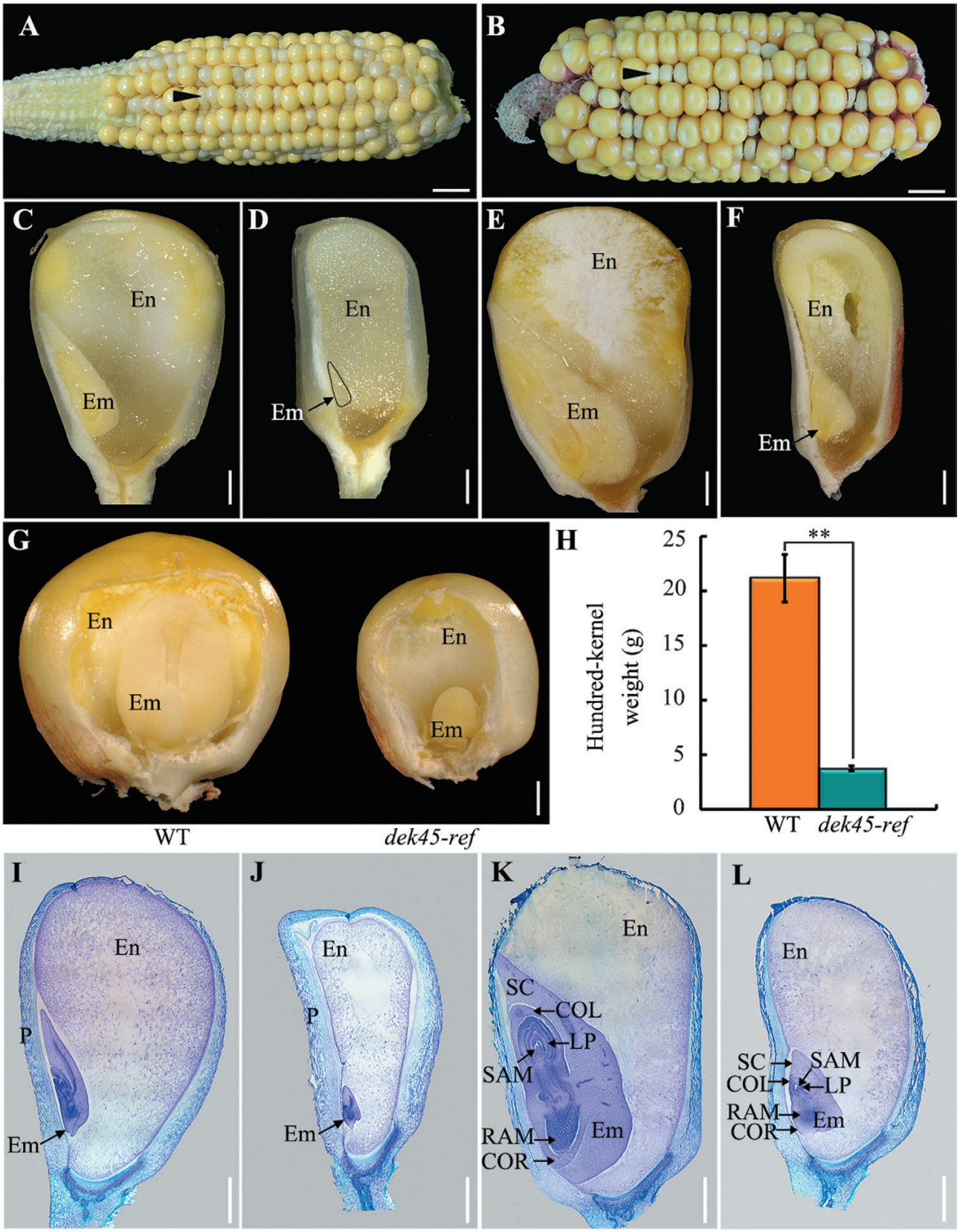

Fig. 1. Phenotypic characterization of *dek45-ref* kernels. (A and B) The self-pollinated *dek45-ref* heterozygote ears at 15 DAP (A) and 25 DAP (B). The arrowhead indicates one of the *dek45-ref* kernels. Scale bars=10 mm. (C–F) Developmental comparisons of dissected WT and *dek45-ref* kernels at 15 and 25 DAP. (C and E) WT kernels at 15 and 25 DAP. (D and F) *dek45-ref* kernels at 15 and 25 DAP. Scale bars=1 mm. (G) The front view of mature WT and *dek45-ref* kernels whose partial pericarp was removed to display an embryo. Scale bars=1 mm. (H) Comparison of the 100-kernel weight of randomly selected mature WT and *dek45-ref* kernels. (I–L) Histological analysis of WT and *dek45-ref* kernels at 15 and 25 DAP. (I and K) WT at 15 and 25 DAP. (J and L) *dek45-ref* kernels at 15 and 25 DAP. Scale bars=1 mm. En, endosperm; Em, embryo; P, pericarp; LP, leaf primordia; RAM, root apical meristem; SAM, shoot apical meristem; SC, scutellum; COL, coleoptile; COR, coleorhiza.

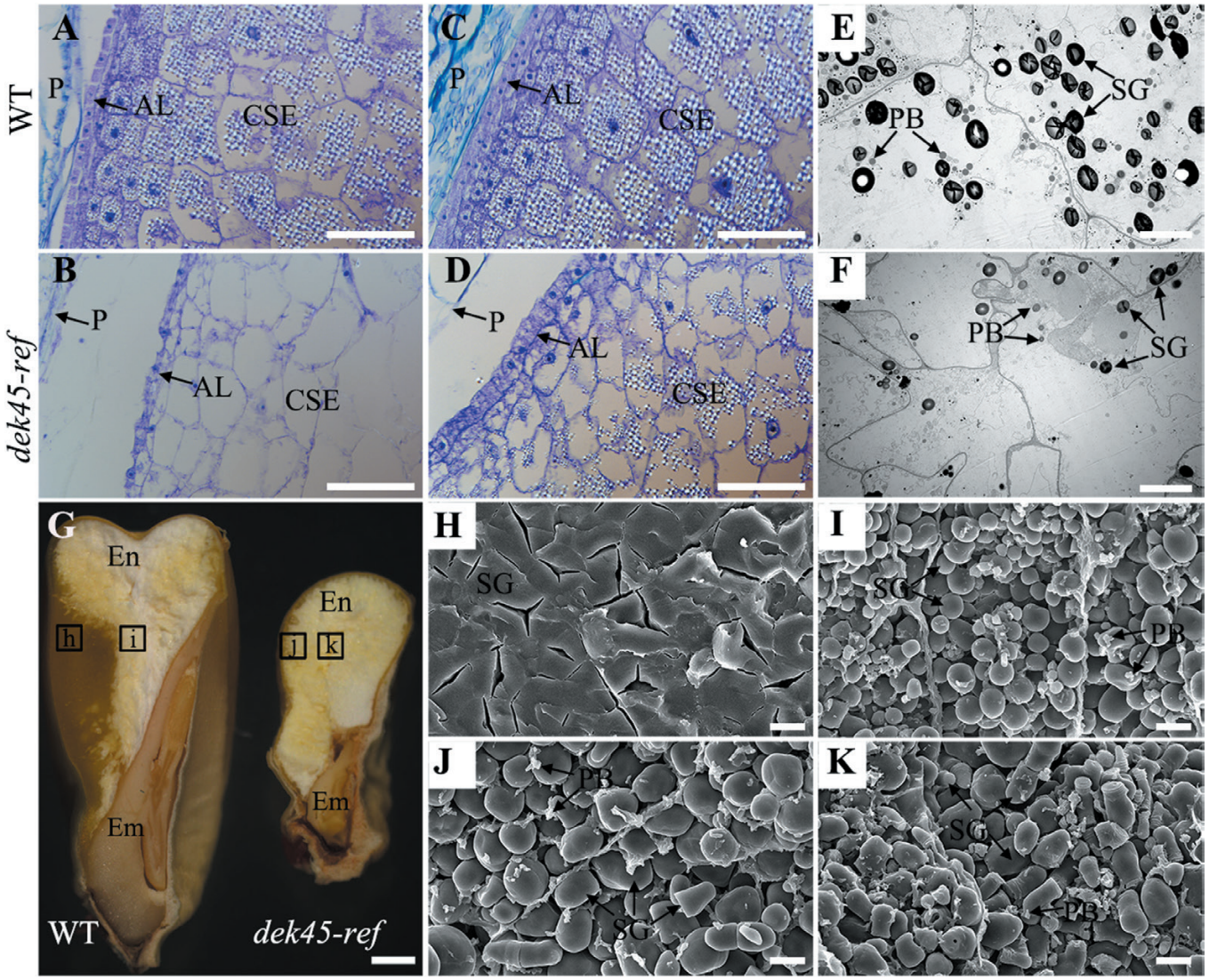

Fig. 2. Comparisons of endosperm in the WT and *dek45-ref* at different developmental stages. (A and B) Histological section analysis of 13 DAP endosperm of WT (A) and *dek45-ref* (B) kernels. Scale bars=100 μm. (C and D) Histological section analysis of 15 DAP endosperm of the WT (C) and *dek45-ref* (D) kernels. Scale bars=100 μm. (E and F) TEM images of 13 DAP endosperms of the WT and *dek45-ref* kernels. Scale bars=10 μm. (G) Longitudinal dissection of WT and *dek45-ref* mature kernels. Scale bars=1 mm. (H–K) SEM images of WT and *dek45-ref* mature endosperm in (G). (H and I) SEM images of WT endosperm in the areas h and i indicated in (G). Scale bars=10 μm. (J and K) SEM images of *dek45-ref* endosperm of in the areas j and k indicated in (G). Scale bars=10 μm. En, endosperm; Em, embryo; P, pericarp; AL, aleurone layer; CSE, central starch endosperm; PB, protein body; SG, starch grain.

were severely defective in *dek45-1* kernels (Fig. 3E). Thus, the *Dek45* gene encoding a PPR protein was responsible for the defective kernel mutant phenotype.

Dek45 *encodes a mitochondrion-targeted PPR-E+ subclass protein*

Genomic DNA structure analysis revealed that *Dek45* contained only one 2595 bp long exon (Fig. 3A). It encoded a novel PPR protein of 864 amino acids with 21 PRR motifs, an E domain and an E+ domain (Fig. 3C; Supplementary Fig. S2). The mutation sites in the *dek45-ref* and *dek45-1* mutants were in the 17th PPR repeat and E domain, respectively (Fig. 3C; Supplementary Fig. S2). The premature stop mutation in *dek45-1* resulted in a truncated protein without E and E+ domains (Fig. 3C; Supplementary Fig. S2). These results suggested that DEK45 belongs to the PPR-E+ subclass, and its E and E+ domains are required for its function.

Previous studies have shown that most PPRs are targeted to either plastids or mitochondria (Lurin *et al.*, 2004; Sosso *et al.*, 2012*a*; Colcombet *et al.*, 2013; Li *et al.*, 2014). To determine the subcellular localization of DEK45, the fused construct p35S:DEK45-GFP was generated and transfected into maize protoplasts. As shown in Fig. 4A, the GFP signal was co-localized with the Mito tracker for mitochondria. To confirm this localization, the construct p35S:DEK45-RFP was transformed into the Arabidopsis marker line MT-GK with GFP-specific expression in mitochondria. The RFP signal was co-localized with the GFP signal in mitochondria of root cells (Fig. 4B), suggesting that the DEK45 protein is targeted to the mitochondria in maize. A gene expression analysis showed that *Dek45* was constitutively expressed in all examined tissues (Fig. 4C).

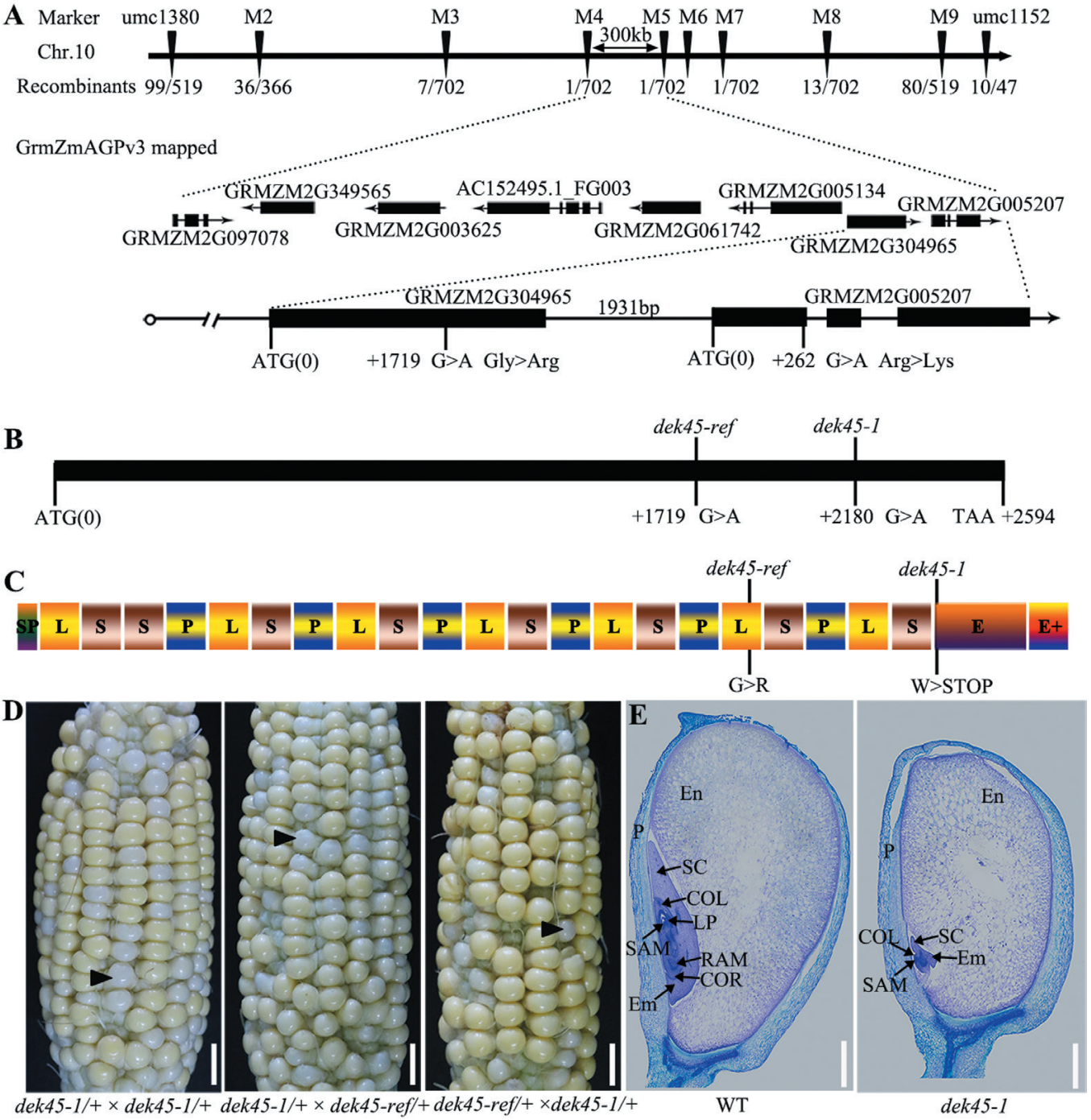

Fig. 3. Map-based cloning and identification of *Dek45*. (A) Fine mapping of the *Dek45* locus. The *Dek45* locus was mapped to a 300 kb region by markers M4 and M5 on chromosome 10, which contains eight candidate genes. The molecular markers and number of recombinants are indicated. The structure and mutation site of the two candidate genes are indicated. (B) Gene structure of *Dek45* and mutation sites in the *Dek45* gene. (C) Schematic diagram of DEK45 protein with a total of 21 PPR domains (P, L, and S), E, and E+ motifs. The mutation sites of amino acid change are indicated. SP, signal peptide. (D) Heterozygous *dek45-ref* and *dek45-1* were used in an allelism test of *Dek45*. The black arrow indicates the mutant kernel. Scale bars=1 cm. (E) Histological analysis of WT and *dek45-1* kernels at 15 DAP. Scale bars=1 mm. En, endosperm; Em, embryo; P, pericarp; LP, leaf primordia; RAM, root apical meristem; SAM, shoot apical meristem; SC, scutellum; COL, coleoptile; COR, coleorhiza.

DEK45 is required for C-to-U RNA editing of multiple mitochondrial transcripts

To investigate the function of *Dek45*, we used gene-specific primers to examine 35 protein-coding mitochondrial genes as described previously (Liu *et al.*, 2013). The results showed that the editing of three C-to-U editing sites, *cox3*-314, *nad2*-26, and *nad5*-1916, in *dek45-ref* was completely abolished (Fig. 5A). Normally, the *cox3*-314 RNA editing site is 95% C-to U-edited, and the *nad2*-26 and *nad5*-1916 editing sites are completely edited. Surprisingly, the editing ratio of *nad5*-1901 was increased in *dek45-ref* (Fig. 5A). We then analyzed these editing sites in the *dek45-1* mutant. RNA editing at the two editing sites *nad2*-26 and *nad5*-1916 was

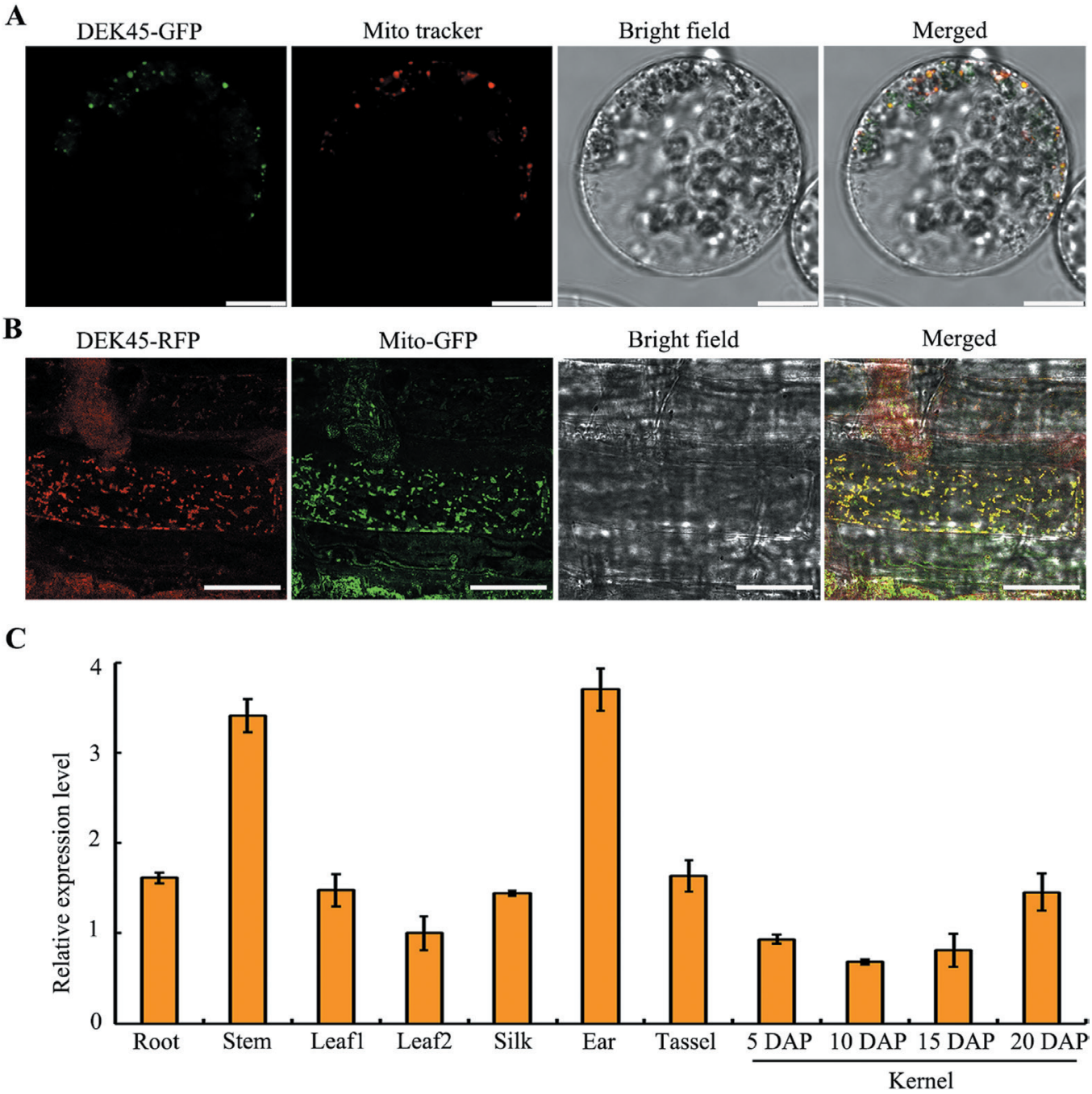

Fig. 4. Subcellular localization of DEK45 and expression pattern of *Dek45*. (A) Fluorescence signals of transiently expressed DEK45–GFP in maize protoplasts. Mitochondria are marked by Mito Tracker (red). Scale bars=10 μm. (B) Subcellular localization of DEK45 protein in the Arabidopsis marker line of mitochondria. The T_1 transgenic line roots were used for imaging by confocal microscopy. The fluorescence signals of expressed DEK45–RFP in the Arabidopsis marker line are shown in red. The Arabidopsis marker line (MT-GK) has a specially expressed GFP in mitochondria, which is marked as Mito-GFP. Scale bars=25 μm. (C) The expression profiles of *Dek45* in a variety of organs and maize kernels at different developmental stages. Leaf1, juvenile leaves; Leaf2, mature leaves; DAP, days after pollination. The RNA levels were normalized to that of the maize *ZmActin* gene (GRMZM2G126010). Values are means of three technical replicates and three biological repeats. Error bars represent the SD.

also completely abolished (Fig. 5A). At the *cox3*-314 site, the RNA editing ratio was reduced to 20% (Fig. 5A). At *nad5*-1901, the editing ratio was increased to 70% (Fig. 5A). These data suggested that the DEK45 protein is necessary for RNA editing at *cox3*-314, *nad2*-26, *nad5*-1901, and *nad5*-1916 in maize.

The defective editing at *cox3*-314, *nad2*-26, *nad5*-1901, and *nad5*-1916 in *dek45-ref* and *dek45-1* resulted in an amino acid replacement compared with the WT (Fig. 5A). The DEK45 target sites of the amino acids at positions 6 and 1′ were analyzed using a previously described method (Barkan *et al.*, 2012; Takenaka *et al.*, 2013*a*). The sequences around the *cox3*-314, *nad2*-26, and *nad5*-1916 RNA editing sites were highly conserved with putative recognition sites (Fig. 5B), indicating that DEK45 is important for RNA editing at these four sites in mitochondria.

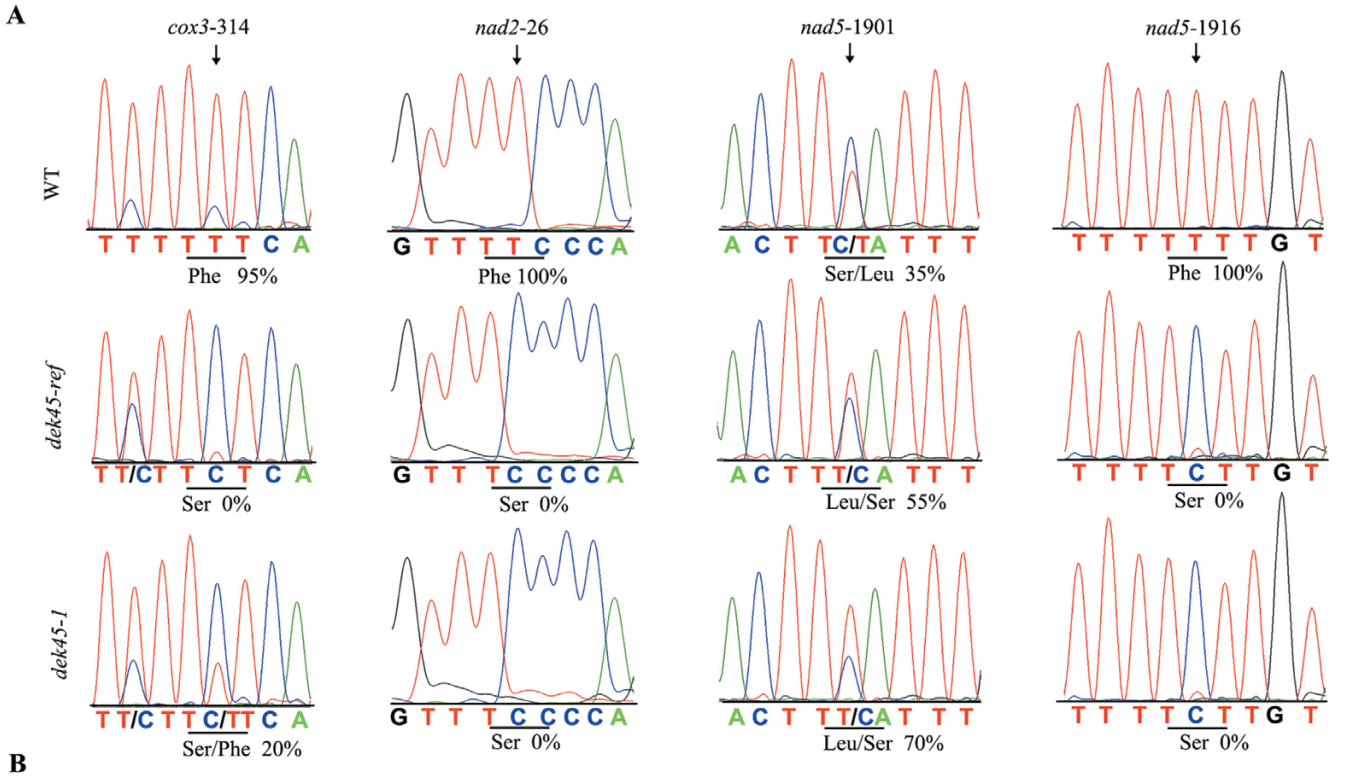

B

Motif	L	S	S	P	L	S	P	L	S	P	L	S	P	L	S	P	L	S	P	L	S
	21	20	19	18	17	16	15	14	13	12	11	10	9	8	7	6	5	4	3	2	1
aa6	L	N	N	N	A	S	G	A	T	N	S	N	N	G	S	N	A	S	N	V	A
aa1'	T	D	D	D	D	N	S	D	N	D	D	D	D	D	E	D	D	D	N	Q	D
A	0.20	0.15	0.15	0.09	0.25	0.70	0.25	0.25	0.64	0.09	0.25	0.15	0.09	0.25	0.25	0.09	0.25	0.06	0.08	0.27	0.09
C	0.32	0.23	0.23	0.25	0.25	0.14	0.25	0.25	0.06	0.25	0.25	0.23	0.25	0.25	0.25	0.25	0.25	0	0.55	0.21	0.07
G	0.00	0.07	0.07	0.14	0.25	0.04	0.25	0.25	0.15	0.14	0.25	0.07	0.14	0.25	0.25	0.14	0.25	0.85	0.08	0.09	0.70
U	0.48	0.55	0.55	0.52	0.25	0.13	0.25	0.25	0.16	0.52	0.25	0.55	0.52	0.25	0.25	0.52	0.25	0.10	0.28	0.42	0.14

position	-24	-23	-22	-21	-20	-19	-18	-17	-16	-15	-14	-13	-12	-11	-10	-9	-8	-7	-6	-5	-4	-3	-2	-1	Edit	1	2	3	4
cox3-314	U	U	U	U	U	G	C	U	U	U	U	U	U	U	U	G	G	G	C	U	U	U	U	U	C	U	C	A	U
nad2-26	U	G	U	U	C	A	A	U	C	U	U	U	U	U	U	U	A	G	C	G	G	U	U	U	C	C	C	C	U
nad5-1916	G	U	U	U	A	A	C	U	U	C	A	U	U	U	G	U	G	A	C	C	U	U	U	U	C	U	U	G	U

Fig. 5. DEK45 is required for *cox3*-314, *nad2*-26, *nad5*-1901, and *nad5*-1916 C-to-U editing in maize mitochondria. (A) Analysis of RNA editing in *cox3*, *nad2*, and *nad5* transcripts of developing kernels in the WT, *dek45-ref*, and *dek45-1*. The arrow marks the editing site. The amino acid encoded is indicated on the bottom, and the editing efficiency is presented under each target site. (B) Prediction and alignment of DEK45 to editing sites in the mitochondrial targets. Prediction of DEK45 target sites of the amino acids at positions 6 and 1' with the coding rule. The probability of each nucleotide binding a DEK45 PPR element is given in the bottom panel, and nucleotides matching the DEK45 RNA recognition site sequences are indicated.

DEK45 recognizes and directly bind to cox3, nad2, *and* nad5 *transcripts*

In the *dek45-ref* mutant, the C-to-U editing at *cox3*-314, *nad2*-26, and *nad5*-1916 was completely abolished, implying that the three transcripts may be targets of DEK45. To investigate whether DEK45 directly binds to these transcripts, an RNA EMSA was carried out. Because the amino acids at positions 6 and 1′ are essential in PPR protein target sites (Barkan *et al.*, 2012; Takenaka *et al.*, 2013*a*), we predicted the DEK45 recognition sequences (Fig. 5B). Three RNA probes (base pairs –29 upstream to +4 downstream of the RNA editing site of *cox3*, *nad2*, and *nad5*) that included 35 nucleotides surrounding the three RNA editing sites were designed and biotin labeled (Fig. 6A). Shifted bands were detected when DEK45–GST was incubated with the RNA probes, but were not identified when the RNA probes were incubated with GST (Fig. 6B–D). The competition assay further showed that the shifted bands distinctly decreased as the competitor concentration increased and the labeled RNA probes increased (Fig. 6B–D). Thus, DEK45 can directly bind *cox3*, *nad2*, and *nad5* transcripts and is necessary for RNA editing at *cox3*-314, *nad2*-26, and *nad5*-1916 in maize.

The activities of mitochondrial complexes I and IV are reduced in the dek45-ref *mutant*

The *nad2* and *nad5* genes encode complex I subunits NAD2 and NAD5, respectively. The *cox3* gene encodes subunit III of the COX that is part of complex IV of the ETC. Thus, the editing defects at *cox3*-314, *nad2*-26, *nad5*-1901, and *nad5*-1916 in *dek45-ref* might affect complex I and IV activity. Mitochondrial complexes were isolated from 15 DAP kernels without pericarp and separated by BN-PAGE. Analyses revealed that the abundances of complexes I and IV decreased dramatically in the *dek45-ref* and *dek45-1* mutants compared

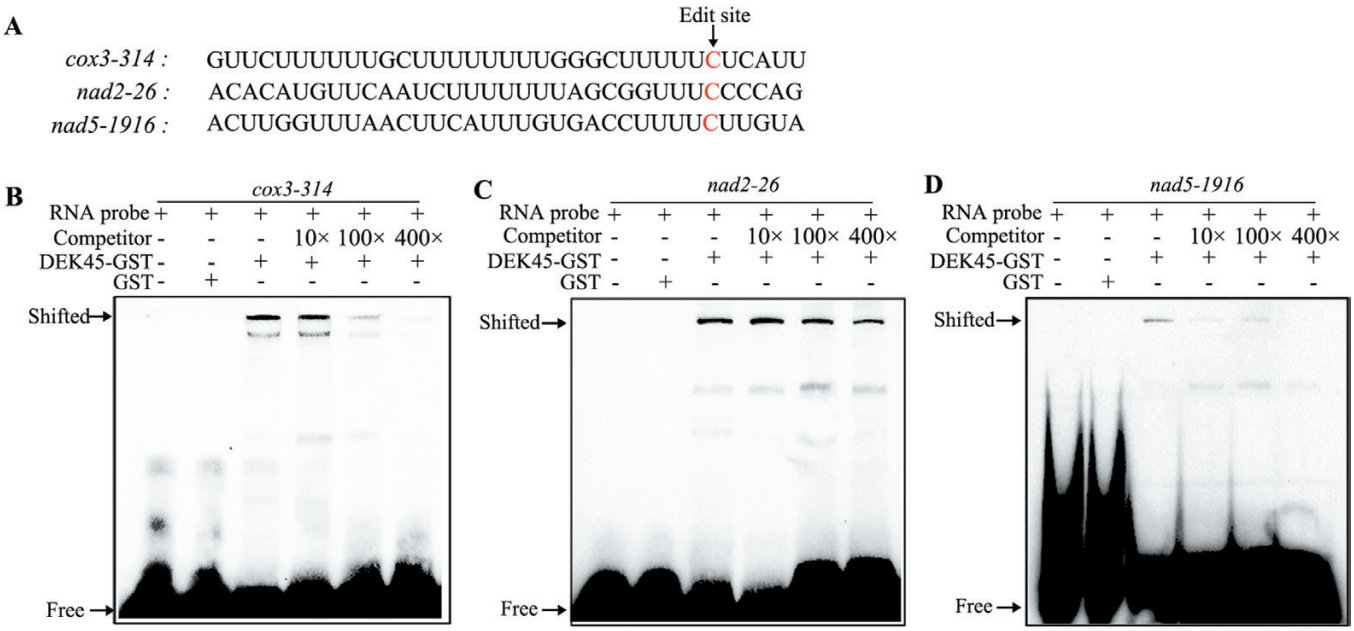

Fig. 6. DEK45 recognizes and directly binds *cox3*, *nad2*, and *nad5* transcripts. (A) Nucleotide sequence of RNA probes. Edited sites are indicated in red. (B) RNA EMSAs indicated that DEK45 directly binds to *cox3* transcripts that surround the *cox3* edited site. Unlabeled probe was used as a competitor, and GST was used as a negative control. Black arrows show the shifted bound and free RNA probe. (C) RNA EMSAs indicated that DEK45 directly binds to *nad2* transcripts that surround the *nad2* edited site. Unlabeled probe was used as a competitor, and GST was used as a negative control. The shifted bound and free RNA probesw are indicated by black arrows. (D) RNA EMSAs indicated that DEK45 directly binds to *nad5* transcripts that surround the *nad5* edited site. Unlabeled probe was used as a competitor, and GST was used as a negative control. The shifted bound and free RNA probes are indicated by black arrows.

with the WT (Fig. 7A). We then investigated the activities of mitochondrial complexes I, II, III, and IV in *dek45-ref* kernels. The activities of complexes I and IV decreased dramatically, but those of complexes II and III increased noticeably in the *dek45-ref* mutant (Fig. 7B). The results suggested that the editing defects at *cox3*-314, *nad2*-26, *nad5*-1901, and *nad5*-1916 in the mutant kernels affected complex I and IV assembly and led to decreased activities of these complexes in the mitochondrial respiratory chain.

Mitochondrial ultrastructure was altered and alternative respiratory pathway activities were increased in the dek45 *mutant*

To determine the functions of *Dek45* in mitochondria, we analyzed the structure of mitochondria in *dek45-ref* and *dek45-1* mutant endosperm at 11 DAP. The WT had normal mitochondria with densely folded inner membranes and distinct cristae (Fig. 7C), whereas the mitochondria of *dek45-ref* and *dek45-1* had large internal spaces and lacked obvious membrane structures (Fig. 7C), implying that DEK45 is required for mitochondrial structure and function during kernel development.

Besides classical ETCs, plants have evolved an alternative respiratory pathway. The alternative oxidase (*Aox*) genes are usually used as markers for the alternative respiratory pathway in the mitochondrial ETC. There are three *Aox* genes, *Aox1* (AC233960.1_FG002), *Aox2* (GRMZM2G125669), and *Aox3* (GRMZM2G074743), in the maize genome. Because the *dek45* mutant appeared to reduce mitochondrial complex I and IV activity, we examined *Aox* transcript accumulation in *dek45-ref* by qRT–PCR. The results showed that *Aox* gene transcript levels, especially that of *Aox2*, were noticeably higher in the *dek45-ref* mutant than in the WT (Fig. 7D). These results indicated that the respiration function of *dek45-ref* mitochondria is severely impaired because of the decrease in complex I and IV activity, which induces the alternative respiratory pathway in the *dek45-ref* mutant.

ROS were overproduced and PCD was initiated early in dek45-ref *endosperm*

ROS production is mainly caused by the mitochondrial ETC complexes I and III (Gill and Tuteja, 2010). Thus, we analyzed the H_2O_2 and O_2^- levels in *dek45-ref* and the WT at 11, 13, and 15 DAP by DAB and NBT staining, respectively. The endosperm of *dek45-ref* accumulated much more ROS than that of the WT (Fig. 8A–D). Furthermore, ROS accumulation was found near the cavity in the *dek45-ref* endosperm (Fig. 8A, C).

To understand the cavity formation phenotype, we performed TUNEL assays on the WT and *dek45-ref* using longitudinal sections of 11, 13, and 15 DAP kernels. No TUNEL-positive signal was detected at 11 DAP in WT or *dek45-ref* endosperm nuclei (Supplementary Fig. S3). Interestingly, strong TUNEL-positive signals started to be detected at 13 DAP in *dek45-ref* endosperm nuclei, but no TUNEL-positive signal was detected in WT endosperm at the same stage (Fig. 9). At 15 DAP, WT endosperm showed weak TUNEL-positive signals close to the pericarp, whereas the *dek45-ref* mutant showed strong TUNEL-positive signals in the central region of the starchy endosperm near the cavity (Fig. 9), implying that nuclear DNA fragmentation started earlier in *dek45-ref* endosperm cells than in the WT. The cavity

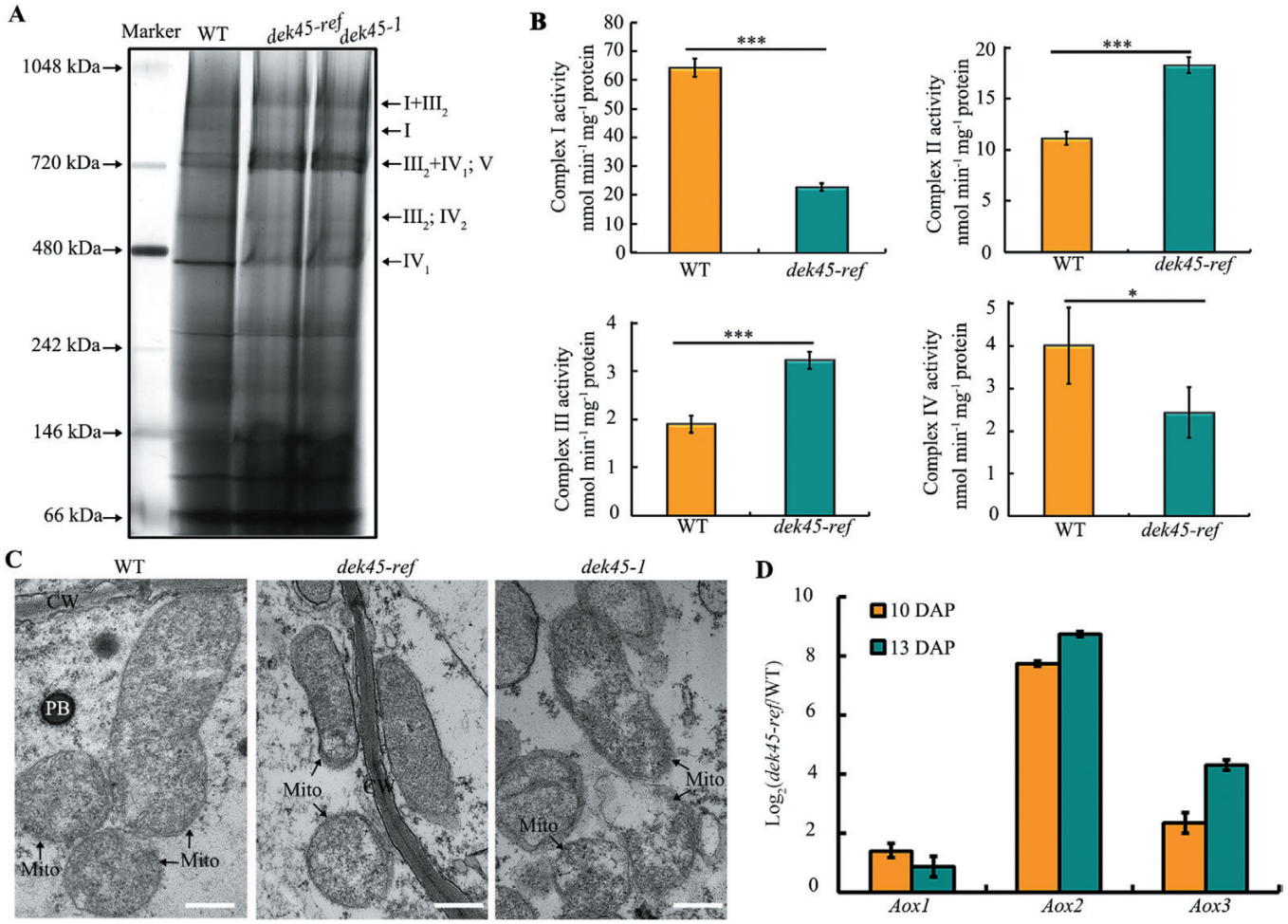

Fig. 7. Comparison of mitochondrial complexes, ultrastructure, and alternative respiratory pathways between the WT and mutants. (A) The BN-PAGE analyses of mitochondrial complexes. The BN-PAGE gels were stained with Coomassie Brilliant Blue (CBB). (B) Activity analyses of four mitochondrial complexes. Values are means of three biological replicates. Error bars represent the SD. Significant differences are indicated. *P<0.05, **P<0.01, ***P<0.001 (Student's t-test). (C) TEM analysis of mitochondrial ultrastructure in 11 DAP endosperm of WT, *dek45-ref*, and *dek45-1*. Mito, mitochondria; PB, protein body; CW, cell wall. Scale bars=500 nm. (D) qRT–PCR analysis of *Aox* gene expression in endosperm at 10 and 13 DAP. Values and bars represent the mean and the SD of three biological replicates, respectively. The RNA levels were normalized to that of the maize *ZmActin* gene (GRMZM2G126010).

in the central region of the endosperm might be caused by abnormal PCD in *dek45-ref*.

The cysteine proteinase and metacaspases are involved in PCD (Suarez *et al.*, 2004; Takahashi *et al.*, 2015). To verify the initiation of PCD in *dek45-ref* mutant endosperm, we examined the expression levels of cysteine proteinase and metacaspase genes. Their expression levels were increased in the *dek45* mutant at 11, 13, and 15 DAP (Supplementary Fig. S4), suggesting that *dek45-ref* endosperm PCD started earlier than in the WT.

Genes were differentially expressed between the WT and dek45-ref

To explain the developmental defects at the gene expression level, RNA-seq analysis was performed with total RNA isolated from WT and *dek45-ref* mutant endosperms at 10 DAP. In total, 1150 genes showed significantly altered expression between the WT and *dek45-ref* mutant (Fig. 10A). To identify metabolic pathways in which the DEGs were enriched, we performed Gene Ontology (GO) classification and pathway analysis using the Kyoto Encyclopedia of Genes and Genomes (KEGG) pathway database (Fig. 10B, C). The largest category was biological process, with 10 subcategories, namely: response to inorganic substance; starch biosynthetic process; response to metal ion; response to stimulus; response to chemical; glycogen biosynthetic process; transition metal ion transport; glycogen metabolic process; energy reserve metabolic process; and protein refolding. The second largest was molecular function with: nutrient reservoir activity; peptidase inhibitor activity; peptidase regulator activity; endopeptidase inhibitor activity; endopeptidase regulator activity; enzyme inhibitor activity; glucose-1-phosphate adenylyltransferase activity; organic anion transmembrane transporter activity; and cellular component (Fig. 10B). A total of 739 DEGs were classified into 120 pathways, 22 of which were significantly enriched (P<0.05). Among the 22 pathways, the extremely significant pathways were biosynthesis of secondary metabolites, followed by glutathione metabolism pathways, isoflavonoid biosynthesis, and phenylpropanoid biosynthesis (Fig. 10C). Notably, many genes functioning in nutrient

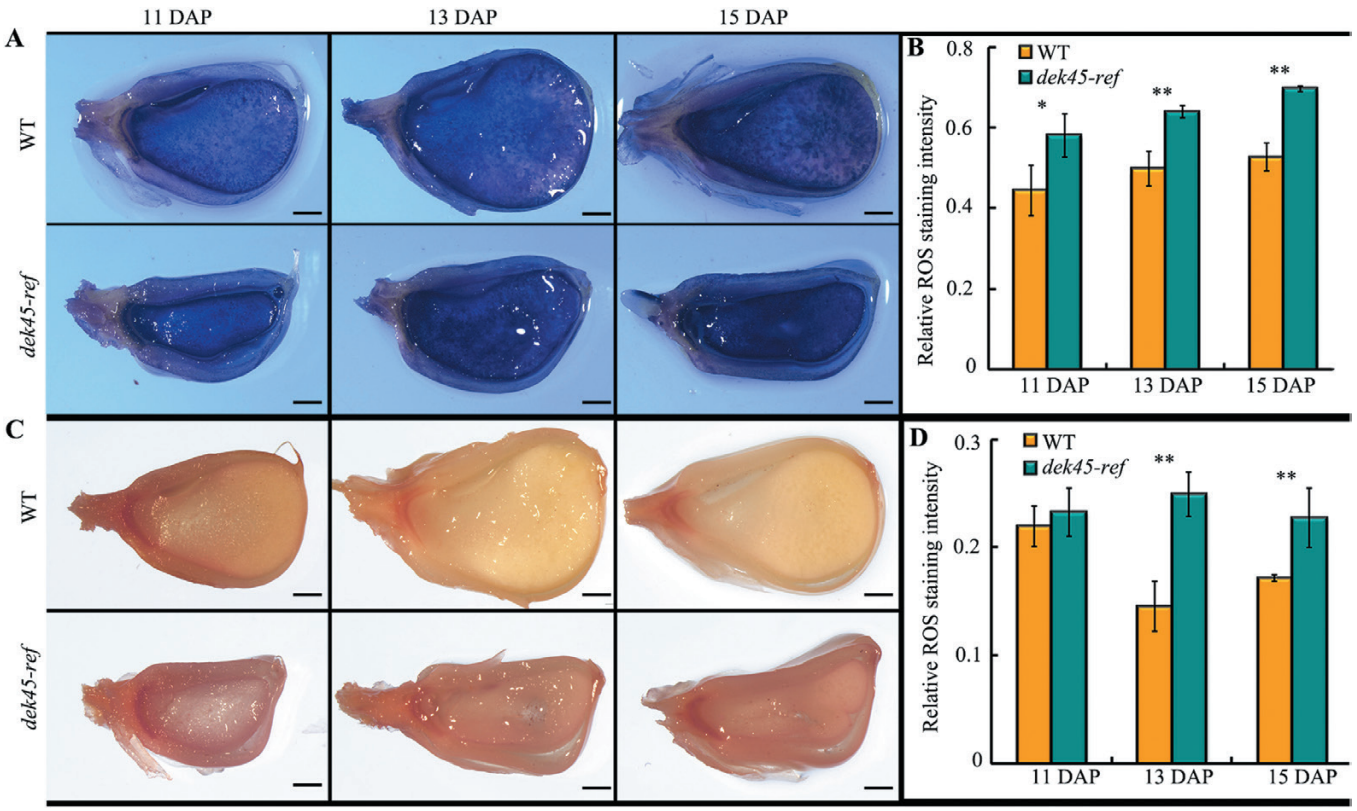

Fig. 8. Abnormal accumulation of ROS in *dek45-ref* endosperm. (A) NBT staining for the detection of superoxide (O_2^-) in endosperm of the WT and *dek45-ref* at 11, 13, and 15 DAP. Scale bars=1 mm. (B) Relative NBT staining intensity in endosperm of the WT and *dek45-ref* at the indicated developmental stage. (C) DAB staining for the detection of hydrogen peroxide (H_2O_2) in endosperm of the WT and *dek45-ref* at 11, 13, and 15 DAP. Scale bars=1 mm. (D) Relative DAB staining intensity in endosperm of the WT and *dek45-ref* at the indicated developmental stages. Values and bars represent the mean and the SD of more than five biological replicates, respectively. Significant differences are indicated. *P<0.05, **P<0.01 (Student's t-test).

storage activity and starch biosynthesis were markedly down-regulated in *dek45-ref* (Fig. 10D).

Discussion

The E+ PPR protein DEK45 is essential for post-transcriptional processing of cox3, nad2, *and* nad5 *transcripts in maize*

PPR proteins play an essential role in post-transcriptional processes in mitochondria and chloroplasts, including RNA editing, splicing and cleavage, and translation (Schmitz-Linneweber and Small, 2008). So far, several *Dek* genes have been reported in previous studies; to investigate the relationships between the DEK45 and other DEK proteins, the phylogenetic tree was constructed (Supplementary Fig. S5). DEK45 is more closely related to DEK36, DEK39, and DEK10 (Supplementary Fig. S5), and they all belong to the PLS-type PPR protein subfamily. They are involved in RNA editing in mitochondria and maize kernel development (Qi *et al.*, 2017; Wang *et al.*, 2017; Li *et al.*, 2018), suggesting that their functions are conserved in maize. In this study, we identified the E+ subgroup PPR protein DEK45 localized to mitochondria in maize (Fig. 4A, B). *Dek45* loss of function caused kernel defects and embryo lethality in maize (Fig. 3D). The *dek45-ref* mutant has a nucleotide change resulting in an amino acid replacement (Gly to Arg) at the 21st amino acid of the 17th PPR motif (L motif) (Fig. 3B, C; Supplementary Fig. S2). The amino acid alignment of maize DEK45 with similar PPR proteins in other plant species showed that the Gly residue was highly conserved (Supplementary Fig. S2). Previous studies have shown that the Gly residue is highly conserved in L motifs (Lurin *et al.*, 2004; Wang *et al.*, 2017). Therefore, the Gly residue in the α-helices of the L motif is required for PPR protein function. The single point mutation in *dek45-1* led to a premature stop codon in *Dek45*, resulting in the loss of the E and E+ domains in DEK45. The studies on EMP5, EMP9, and MEF3 revealed that the E domain but not the E+ domain is essential for RNA editing (Verbitskiy *et al.*, 2012; Liu *et al.*, 2013; Yang *et al.*, 2017), which in combination with our results suggests that the E domain is an important functional domain in E/E+ subgroup PPR proteins.

Bioinformatics and structural analyses indicated that RNA substrates of PPR proteins could be identified in a motif sequence-specific manner (Barkan *et al.*, 2012; Takenaka *et al.*, 2013*a*; Yin *et al.*, 2013). However, to our knowledge, very few studies have shown direct evidence for the recognition and binding between PPR proteins and their targets. In our study, we confirmed the binding capacity between DEK45 and target RNAs (Fig. 6B–D), which provides very important information for the illumination of the functional mechanism of PPR proteins. Editing at the *cox3*-314, *nad2*-26, and *nad5*-1916 sites in *dek45-ref* was completely abolished, but the editing ratio at *nad5*-1901 was increased (Fig. 5A), suggesting that DEK45 is

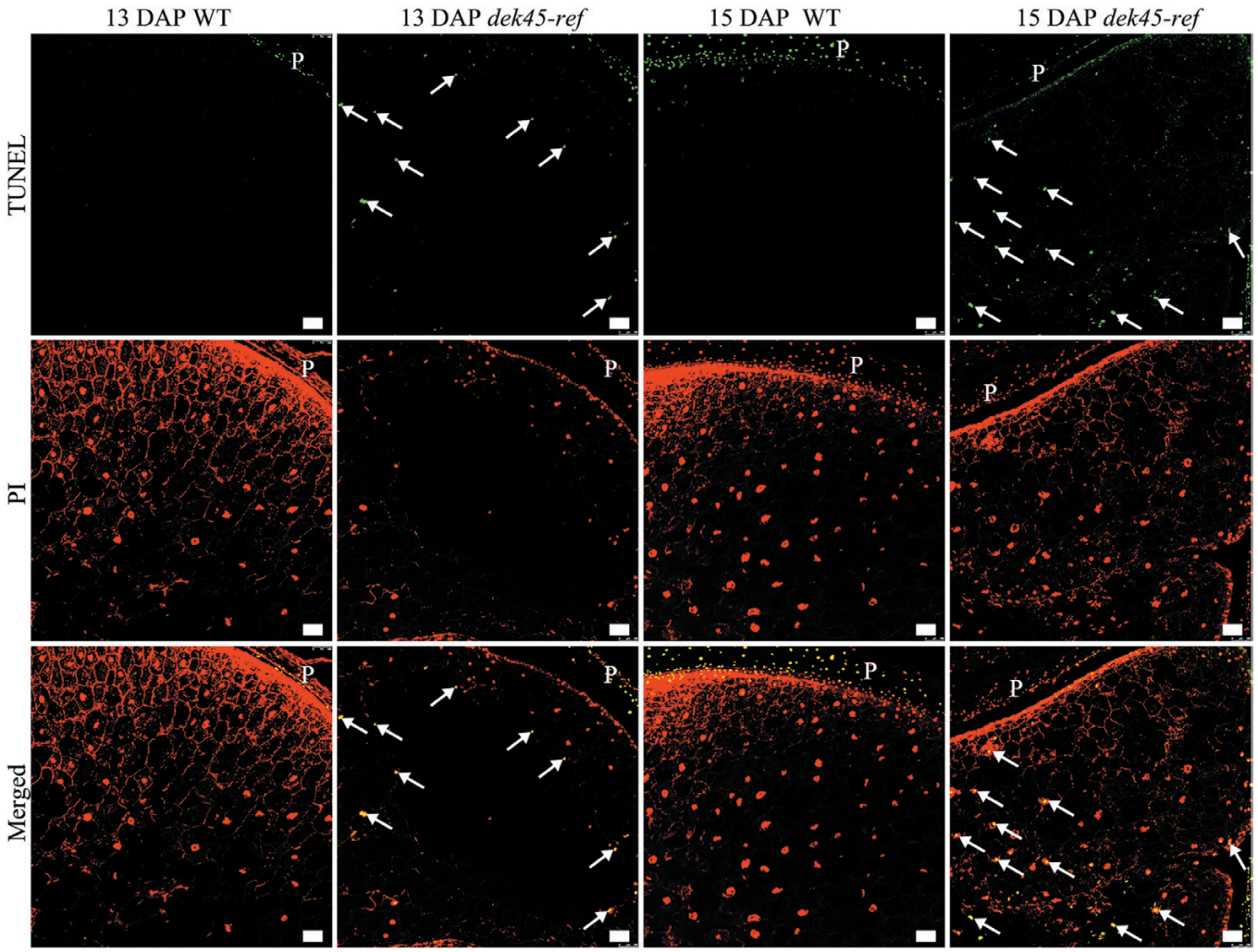

Fig. 9. Earlier PCD in *dek45-ref* endosperm. Nuclear DNA fragmentation in WT and *dek45-ref* endosperm at 13 and 15 DAP was detected by TUNEL assay. Green indicates the TUNEL signals. Red is PI showing the nuclei. Yellow is a merge of TUNEL-detected nuclei and PI-detected nuclei. The white arrowheads show examples of a positive signal. P, pericarp. Scale bars=100 μm.

involved in multiple editing events. MEF13, the Arabidopsis ortholog of DEK45, is responsible for editing at eight target sites (*ccmFc*-50, *nad2*-59, *nad5*-1665, *nad5*-1916, *nad7*-213, *cox3*-314, *nad4*-158, and *ccmFc*-415) (Glass *et al.*, 2015). However, we did not find RNA editing at *ccmFc*-50, *nad7*-213, and *nad5*-1665 in WT or *dek45-ref* mitochondria in maize. Sequence alignment showed that the maize *nad2*-26, *cox3*-314, and *nad5*-1916 editing positions are consistent with Arabidopsis *nad2*-53, *cox3*-314, and *nad5*-1916 transcripts, respectively. Interestingly, the *nad5*-1901 editing ratio was increased in *dek45-ref*, which was not be found in Arabidopsis *mef13*. Taken together, DEK45 has divergent functions in regulating mitochondrial RNA metabolism between maize and Arabidopsis.

Post-transcriptional processing of cox3, nad2, *and* nad5 *transcripts is required for mitochondrial functions in maize*

In maize, 22 proteins in the ETC are encoded by mitochondrial genes, which include nine subunits (NAD1, 2, 3, 4, 4L, 5, 6, 7, and 9) of complex I, one subunit (cob) of complex III, three subunits (COX 1, 2, and 3) of complex IV, four subunits (CCMB, C, FN, and FC) of cytochrome *c*, and five subunits (ATP 1, 4, 6, 8, and 9) of complex V (Clifton *et al.*, 2004). Here, we found that editing defects at *cox3*-314, *nad2*-26, *nad5*-1901, and *nad5*-1916 in the *dek45* mutant resulted in an amino acid change compared with the WT (Fig. 5A). *nad2* and *nad5* encode complex I subunits NAD2 and NAD5, respectively, while *cox3* encodes complex IV subunit COX3. The abundance and activities of complexes I and IV were dramatically decreased in the *dek45* mutant, but the activities of complexes II and III were noticeably increased (Fig. 7A, B). These changes might lead to dysfunction of the mitochondria and damage of the mitochondrial ultrastructure (Fig. 7C, D). NAD2 and NAD5 are essential for the assembly and activity of complex I. The splicing efficiency of the mitochondrial *nad2* intron was affected by EMP16, EMP10, DEK37, PPR-SMR1, or EMP12 (Xiu *et al.*, 2016; Cai *et al.*, 2017; Dai *et al.*, 2018; Chen *et al.*, 2019; Sun *et al.*, 2019). Loss of PPR78 led to a reduction in the steady-state level of the mitochondrial *nad5* mature mRNA (Zhang *et al.*, 2017). These mutations reduce the assembly and activity of complex I. COX3 is also critical for mitochondrial functions. For example, RNA editing defects in *cox3* resulted in reduced COX activity and inhibition of the mitochondrial

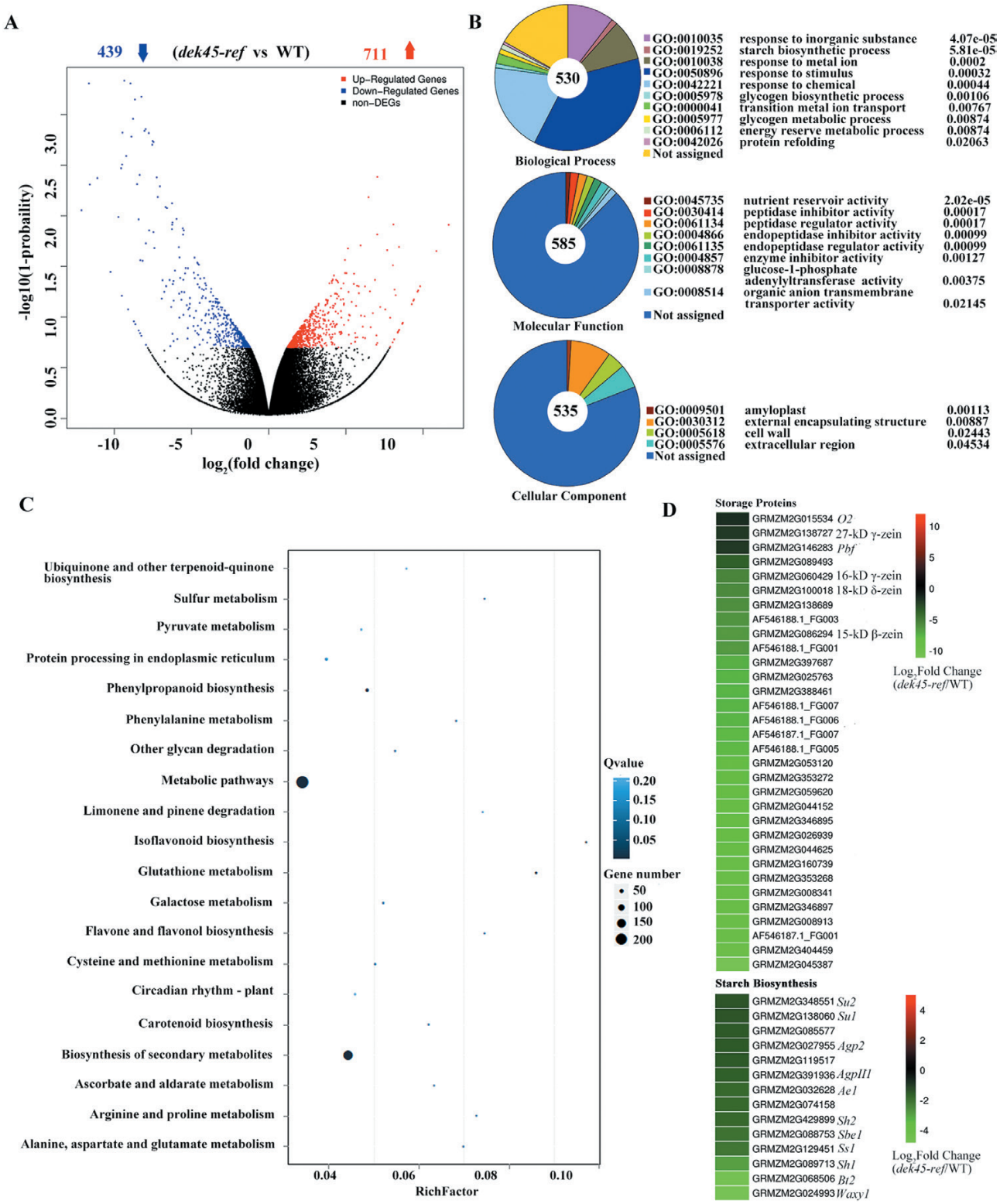

Fig. 10. Identification of differentially expressed genes (DEGs) between the WT and *dek45-ref* by RNA-seq. (A) The number of DEGs between the *dek45-ref* mutant and WT. Fold change ≥2; –log10(1–probability) ≥0.8. Blue and red arrows represent the number of down- and up-regulated genes in *dek45-ref* compared with the WT, respectively. (B) The most significantly related GO terms of the functional annotated DEGs, $P<0.05$. (C) Pathway functional enrichment of DEGs. The *x*-axis represents the enrichment factor and the *y*-axis represents the pathway name. (D) Heat maps of differentially expressed genes involved in storage protein and starch biosynthesis.

respiratory pathway (Tang *et al.*, 2010). Thus, we suggest that the NAD2-9 (Phe), NAD5-639 (Phe). and COX3-105 (Phe) amino acids correctly encoded at the editing site are required for mitochondrial function in maize, and the editing at *cox3*-314, *nad2*-26, *nad5*-1901, and *nad5*-1916 is critical to mitochondrial functions.

Mitochondrial dysfunction affects kernel development

As well as the classical oxidative phosphorylation system, the alternative respiratory pathways play an important role in plant respiratory electron transport in mitochondria (Eubel *et al.*, 2004). Reduced assembly and activity of mitochondrial complexes increases the AOX protein content and *AOX* transcript levels (Zsigmond *et al.*, 2008; Sosso *et al.*, 2012*b*; Xie *et al.*, 2016; Xiu *et al.*, 2016; Ren *et al.*, 2017). In the *dek45* mutant, *AOX* transcript levels were increased and more ROS were generated than in the WT, implying that mitochondrial dysfunction leads to cellular redox imbalance and causes ROS overproduction.

The ROS generated in the ETC play a key role in triggering plant PCD (Wu *et al.*, 2015). In d*ek45-ref*, complex I was defective, but ROS accumulation was increased in the endosperm (Fig. 8A–D), which might explain why PCD began earlier in *dek45-ref* endosperm than in the WT (Fig. 9). This is probably caused by ROS overproduction through mitochondrial complex III in *dek45-ref* and is consistent with a previous study in which the ROS generated from complex III play a major role in triggering *mod1* cell death (Wu *et al.*, 2015). Generally, PCD starts in the central region of the endosperm and then spreads to the periphery (Young *et al.*, 1997;Young and Gallie, 2000). In *sh2* endosperm cells, PCD occurs earlier in the central endosperm and progresses outwardly more rapidly than in WT endosperm, which interferes with starch and storage protein synthesis (Young *et al.*, 1997). In *fl4*, accelerated PCD may stop the development of the central starchy endosperm cells (Wang *et al.*, 2014). Similarly, the *dek45-ref* mutant showed a large cavity in the central starchy endosperm that might be caused by early PCD.

In brief, we propose that DEK45 is essential for post-transcriptional processing of *cox3*, *nad2*, and *nad5* transcripts and kernel development in maize. Abnormal DEK45 could not edit its target sites in *cox3*, *nad2*, and *nad5* transcripts, which disrupted the assembly of mitochondrial complexes and led to damage to the mitochondrial ultrastructure. Increased accumulation of ROS in the mutants promoted PCD through the regulation of gene expression and caused defective maize kernels.

Supplementary data

Supplementary data are available at *JXB* online.

Fig. S1. Analysis of paraffin sections of WT and *dek45-ref* kernels at different developmental stages.

Fig. S2. Amino acid alignment of maize DEK45 with homologous PPR proteins in other plant species.

Fig. S3. Nuclear DNA fragmentation was detected in WT and *dek45-ref* endosperm at 11 DAP by TUNEL assay.

Fig. S4. The expression levels of PCD-associated genes.

Fig. S5. Phylogenetic relationships between DEK45 and other maize DEK proteins.

Table S1. Genetic analysis of the kernels in the F_2 population of the segregating ears.

Table S2. Co-segregation analysis of the mutant sites and phenotypes of progenies from wild-type phenotype kernels segregated from self-pollinated *dek45-ref* heterozygous ears.

Table S3. Genotypes of kernels in the crosses between *dek45-ref* and *dek45-1* heterozygote ears were identified by PCR sequencing.

Table S4. Primer sequences used in this study.

Acknowledgements

This work was funded by the National Natural Science Foundation of China (91735301 and 91535109), the National Plant Transgenic Program (2016ZX08003-003), Taishan Scholars Project (ts201712024), funds of Shandong 'Double Tops' Program (SYL2017YSTD03), and a project (dxkt201707) from the State Key Laboratory of Crop Biology. The authors declare no competing financial interests.

Author contributions

XYZ and XSZ conceived the project; RCR, YMW, YJZ, and LLW performed the experiments; RCR and LZ conducted bioinformatics analyses; XL and CZ isolated the *dek45* mutants; and XYZ, RCR, and XSZ wrote the paper.

References

Barkan A, Rojas M, Fujii S, Yap A, Chong YS, Bond CS, Small I. 2012. A combinatorial amino acid code for RNA recognition by pentatricopeptide repeat proteins. PLoS Genetics **8**, e1002910.

Barkan A, Small I. 2014. Pentatricopeptide repeat proteins in plants. Annual Review of Plant Biology **65**, 415–442.

Blokhina O, Fagerstedt KV. 2010. Reactive oxygen species and nitric oxide in plant mitochondria: origin and redundant regulatory systems. Physiologia Plantarum **138**, 447–462.

Cai M, Li S, Sun F, Sun Q, Zhao H, Ren X, Zhao Y, Tan BC, Zhang Z, Qiu F. 2017. *Emp10* encodes a mitochondrial PPR protein that affects the *cis*-splicing of *nad2* intron 1 and seed development in maize. The Plant Journal **91**, 132–144.

Castandet B, Araya A. 2011. RNA editing in plant organelles. Why make it easy? Biochemistry **76**, 924–931.

Chen X, Feng F, Qi W, Xu L, Yao D, Wang Q, Song R. 2017. *Dek35* encodes a PPR protein that affects *cis*-splicing of mitochondrial *nad4* intron 1 and seed development in maize. Molecular Plant **10**, 427–441.

Chen Z, Wang HC, Shen J, Sun F, Wang M, Xu C, Tan BC. 2019. PPR-SMR1 is required for the splicing of multiple mitochondrial introns and interacts with Zm-mCSF1 and is essential for seed development in maize. Journal of Experimental Botany **70**, 5245–5258.

Clifton SW, Minx P, Fauron CM, *et al.* 2004. Sequence and comparative analysis of the maize NB mitochondrial genome. Plant Physiology **136**, 3486–3503.

Colcombet J, Lopez-Obando M, Heurtevin L, Bernard C, Martin K, Berthomé R, Lurin C. 2013. Systematic study of subcellular localization of Arabidopsis PPR proteins confirms a massive targeting to organelles. RNA Biology **10**, 1557–1575.

Dai D, Luan S, Chen X, Wang Q, Feng Y, Zhu C, Qi W, Song R. 2018. Maize *Dek37* encodes a P-type PPR protein that affects *cis*-splicing of mitochondrial *nad2* Intron 1 and seed development. Genetics **208**, 1069–1082.

Dudkina NV, Heinemeyer J, Sunderhaus S, Boekema EJ, Braun HP. 2006. Respiratory chain supercomplexes in the plant mitochondrial membrane. Trends in Plant Science **11**, 232–240.

Eubel H, Heinemeyer J, Sunderhaus S, Braun HP. 2004. Respiratory chain supercomplexes in plant mitochondria. Plant Physiology and Biochemistry **42**, 937–942.

Fujii S, Small I. 2011. The evolution of RNA editing and pentatricopeptide repeat genes. New Phytologist **191**, 37–47.

Gadicherla AK, Stowe DF, Antholine WE, Yang M, Camara AK. 2012. Damage to mitochondrial complex I during cardiac ischemia reperfusion injury is reduced indirectly by anti-anginal drug ranolazine. Biochimica et Biophysica Acta **1817**, 419–429.

Gambino G, Perrone I, Gribaudo I. 2008. A rapid and effective method for RNA extraction from different tissues of grapevine and other woody plants. Phytochemical Analysis **19**, 520–525.

Gechev TS, Van Breusegem F, Stone JM, Denev I, Laloi C. 2006. Reactive oxygen species as signals that modulate plant stress responses and programmed cell death. Bioessays **28**, 1091–1101.

Gill SS, Tuteja N. 2010. Reactive oxygen species and antioxidant machinery in abiotic stress tolerance in crop plants. Plant Physiology and Biochemistry **48**, 909–930.

Glass F, Härtel B, Zehrmann A, Verbitskiy D, Takenaka M. 2015. MEF13 requires MORF3 and MORF8 for RNA editing at eight targets in mitochondrial mRNAs in *Arabidopsis thaliana*. Molecular Plant **8**, 1466–1477.

Ichinose M, Sugita M. 2017. RNA editing and its molecular mechanism in plant organelles. Genes **8**, 5.

Kalyaanamoorthy S, Minh BQ, Wong TKF, von Haeseler A, Jermiin LS. 2017. ModelFinder: fast model selection for accurate phylogenetic estimates. Nature Methods **14**, 587–589.

Katoh K, Misawa K, Kuma K, Miyata T. 2002. MAFFT: a novel method for rapid multiple sequence alignment based on fast Fourier transform. Nucleic Acids Research **30**, 3059–3066.

Kim D, Langmead B, Salzberg SL. 2015. HISAT: a fast spliced aligner with low memory requirements. Nature Methods **12**, 357–360.

Laloi C, Apel K, Danon A. 2004. Reactive oxygen signalling: the latest news. Current Opinion in Plant Biology **7**, 323–328.

Langmead B, Salzberg SL. 2012. Fast gapped-read alignment with Bowtie 2. Nature Methods **9**, 357–359.

Lee K, Han JH, Park YI, Colas des Francs-Small C, Small I, Kang H. 2017. The mitochondrial pentatricopeptide repeat protein PPR19 is involved in the stabilization of *NADH dehydrogenase 1* transcripts and is crucial for mitochondrial function and *Arabidopsis thaliana* development. New Phytologist **215**, 202–216.

Li B, Dewey CN. 2011. RSEM: accurate transcript quantification from RNA-Seq data with or without a reference genome. BMC Bioinformatics **12**, 323.

Li X, Gu W, Sun S, Chen Z, Chen J, Song W, Zhao H, Lai J. 2018. *Defective Kernel 39* encodes a PPR protein required for seed development in maize. Journal of Integrative Plant Biology **60**, 45–64.

Li XJ, Zhang YF, Hou M, *et al*. 2014. *Small kernel 1* encodes a pentatricopeptide repeat protein required for mitochondrial *nad7* transcript editing and seed development in maize (*Zea mays*) and rice (*Oryza sativa*). The Plant Journal **79**, 797–809.

Li XL, Huang WL, Yang HH, Jiang RC, Sun F, Wang HC, Zhao J, Xu CH, Tan BC. 2019. EMP18 functions in mitochondrial *atp6* and *cox2* transcript editing and is essential to seed development in maize. New Phytologist **221**, 896–907.

Liu Y, He J, Chen Z, Ren X, Hong X, Gong Z. 2010. *ABA overly-sensitive 5* (*ABO5*), encoding a pentatricopeptide repeat protein required for *cis*-splicing of mitochondrial *nad2* intron 3, is involved in the abscisic acid response in Arabidopsis. The Plant Journal **63**, 749–765.

Liu YJ, Xiu ZH, Meeley R, Tan BC. 2013. *Empty pericarp5* encodes a pentatricopeptide repeat protein that is required for mitochondrial RNA editing and seed development in maize. The Plant Cell **25**, 868–883.

Lu X, Liu J, Ren W, *et al.* 2018. Gene-indexed mutations in maize. Molecular Plant **11**, 496–504.

Luo C, Long J, Liu J. 2008. An improved spectrophotometric method for a more specific and accurate assay of mitochondrial complex III activity. Clinica Chimica Acta **395**, 38–41.

Lurin C, Andrés C, Aubourg S, *et al.* 2004. Genome-wide analysis of Arabidopsis pentatricopeptide repeat proteins reveals their essential role in organelle biogenesis. The Plant Cell **16**, 2089–2103.

Mühling J, Tiefenbach M, López-Barneo J, *et al.* 2010. Mitochondrial complex II participates in normoxic and hypoxic regulation of α-keto acids in the murine heart. Journal of Molecular and Cellular Cardiology **49**, 950–961.

Nguyen LT, Schmidt HA, von Haeseler A, Minh BQ. 2015. IQ-TREE: a fast and effective stochastic algorithm for estimating maximum-likelihood phylogenies. Molecular Biology and Evolution **32**, 268–274.

Qi W, Tian Z, Lu L, Chen X, Chen X, Zhang W, Song R. 2017. Editing of mitochondrial transcripts *nad3* and *cox2* by Dek10 is essential for mitochondrial function and maize plant development. Genetics **205**, 1489–1501.

Ren X, Pan Z, Zhao H, Zhao J, Cai M, Li J, Zhang Z, Qiu F. 2017. EMPTY PERICARP11 serves as a factor for splicing of mitochondrial *nad1* intron and is required to ensure proper seed development in maize. Journal of Experimental Botany **68**, 4571–4581.

Saha D, Prasad AM, Srinivasan R. 2007. Pentatricopeptide repeat proteins and their emerging roles in plants. Plant Physiology and Biochemistry **45**, 521–534.

Schmitz-Linneweber C, Small I. 2008. Pentatricopeptide repeat proteins: a socket set for organelle gene expression. Trends in Plant Science **13**, 663–670.

Small ID, Peeters N. 2000. The PPR motif—a TPR-related motif prevalent in plant organellar proteins. Trends in Biochemical Sciences **25**, 46–47.

Sosso D, Canut M, Gendrot G, Dedieu A, Chambrier P, Barkan A, Consonni G, Rogowsky PM. 2012*a*. *PPR8522* encodes a chloroplast-targeted pentatricopeptide repeat protein necessary for maize embryogenesis and vegetative development. Journal of Experimental Botany **63**, 5843–5857.

Sosso D, Mbelo S, Vernoud V, *et al.* 2012*b*. PPR2263, a DYW-subgroup pentatricopeptide repeat protein, is required for mitochondrial *nad5* and *cob* transcript editing, mitochondrion biogenesis, and maize growth. The Plant Cell **24**, 676–691.

Suarez MF, Filonova LH, Smertenko A, Savenkov EI, Clapham DH, von Arnold S, Zhivotovsky B, Bozhkov PV. 2004. Metacaspase-dependent programmed cell death is essential for plant embryogenesis. Current Biology **14**, R339–R340.

Sun F, Wang X, Bonnard G, Shen Y, Xiu Z, Li X, Gao D, Zhang Z, Tan BC. 2015. *Empty pericarp7* encodes a mitochondrial E-subgroup pentatricopeptide repeat protein that is required for *ccmFN* editing, mitochondrial function and seed development in maize. The Plant Journal **84**, 283–295.

Sun F, Xiu Z, Jiang R, Liu Y, Zhang X, Yang YZ, Li X, Zhang X, Wang Y, Tan BC. 2019. The mitochondrial pentatricopeptide repeat protein EMP12 is involved in the splicing of three *nad2* introns and seed development in maize. Journal of Experimental Botany **70**, 963–972.

Takahashi H, Yamauchi T, Rajhi I, Nishizawa NK, Nakazono M. 2015. Transcript profiles in cortical cells of maize primary root during ethylene-induced lysigenous aerenchyma formation under aerobic conditions. Annals of Botany **115**, 879–894.

Takenaka M, Verbitskiy D, Zehrmann A, Härtel B, Bayer-Császár E, Glass F, Brennicke A. 2014. RNA editing in plant mitochondria—connecting RNA target sequences and acting proteins. Mitochondrion **19**, 191–197.

Takenaka M, Zehrmann A, Brennicke A, Graichen K. 2013*a*. Improved computational target site prediction for pentatricopeptide repeat RNA editing factors. PLoS One **8**, e65343.

Takenaka M, Zehrmann A, Verbitskiy D, Härtel B, Brennicke A. 2013*b*. RNA editing in plants and its evolution. Annual Review of Genetics **47**, 335–352.

Tang J, Kobayashi K, Suzuki M, Matsumoto S, Muranaka T. 2010. The mitochondrial PPR protein LOVASTATIN INSENSITIVE 1 plays regulatory roles in cytosolic and plastidial isoprenoid biosynthesis through RNA editing. The Plant Journal **61**, 456–466.

Vanlerberghe GC. 2013. Alternative oxidase: a mitochondrial respiratory pathway to maintain metabolic and signaling homeostasis during abiotic and biotic stress in plants. International Journal of Molecular Sciences **14**, 6805–6847.

Verbitskiy D, Merwe JA, Zehrmann A, Härtel B, Takenaka M. 2012. The E-class PPR protein MEF3 of *Arabidopsis thaliana* can also function in mitochondrial RNA editing with an additional DYW domain. Plant & Cell Physiology **53**, 358–367.

Wang G, Qi W, Wu Q, Yao D, Zhang J, Zhu J, Wang G, Wang G, Tang Y, Song R. 2014. Identification and characterization of maize *floury4*

as a novel semidominant opaque mutant that disrupts protein body assembly. Plant Physiology **165**, 582–594.

Wang G, Zhong M, Shuai B, Song J, Zhang J, Han L, Ling H, Tang Y, Wang G, Song R. 2017. E+ subgroup PPR protein defective kernel 36 is required for multiple mitochondrial transcripts editing and seed development in maize and Arabidopsis. New Phytologist **214**, 1563–1578.

Wu J, Sun Y, Zhao Y, *et al.* 2015. Deficient plastidic fatty acid synthesis triggers cell death by modulating mitochondrial reactive oxygen species. Cell Research **25**, 621–633.

Xie T, Chen D, Wu J, Huang X, Wang Y, Tang K, Li J, Sun M, Peng X. 2016. *Growing slowly 1* locus encodes a PLS-type PPR protein required for RNA editing and plant development in Arabidopsis. Journal of Experimental Botany **67**, 5687–5698.

Xiu Z, Sun F, Shen Y, Zhang X, Jiang R, Bonnard G, Zhang J, Tan BC. 2016. EMPTY PERICARP16 is required for mitochondrial *nad2* intron 4 *cis*-splicing, complex I assembly and seed development in maize. The Plant Journal **85**, 507–519.

Yang YZ, Ding S, Wang HC, Sun F, Huang WL, Song S, Xu C, Tan BC. 2017. The pentatricopeptide repeat protein EMP9 is required for mitochondrial *ccmB* and *rps4* transcript editing, mitochondrial complex biogenesis and seed development in maize. New Phytologist **214**, 782–795.

Yin P, Li Q, Yan C, *et al.* 2013. Structural basis for the modular recognition of single-stranded RNA by PPR proteins. Nature **504**, 168–171.

Yoo SD, Cho YH, Sheen J. 2007. Arabidopsis mesophyll protoplasts: a versatile cell system for transient gene expression analysis. Nature Protocols **2**, 1565–1572.

Young TE, Gallie DR. 2000. Regulation of programmed cell death in maize endosperm by abscisic acid. Plant Molecular Biology **42**, 397–414.

Young TE, Gallie DR, DeMason DA. 1997. Ethylene-mediated programmed cell death during maize endosperm development of wild-type and *shrunken2* genotypes. Plant Physiology **115**, 737–751.

Zhang H, Zhang TT, Liu H, Shi Y, Wang M, Bie XM, Li XG, Zhang XS. 2018. Thioredoxin-mediated ROS homeostasis explains natural variation in plant regeneration. Plant Physiology **176**, 2231–2250.

Zhang YF, Suzuki M, Sun F, Tan BC. 2017. The mitochondrion-targeted PENTATRICOPEPTIDE REPEAT78 protein is required for *nad5* mature mRNA stability and seed development in maize. Molecular Plant **10**, 1321–1333.

Zsigmond L, Rigó G, Szarka A, Székely G, Otvös K, Darula Z, Medzihradszky KF, Koncz C, Koncz Z, Szabados L. 2008. Arabidopsis PPR40 connects abiotic stress responses to mitochondrial electron transport. Plant Physiology **146**, 1721–1737.